Linköping University | Department of Electrical Engineering
Master's thesis, 30 ECTS | Elektroteknik
2023 | LIU-ISY/LITH-EX-A--23/001--SE

Second Life Applications for Degraded EV Batteries

– Evaluating Benefits Based on Remaining Useful Life and Battery Configurations

Elis Sandberg

Supervisor : Daniel Jung
Examiner : Christofer Sundström

Linköpings universitet
SE–581 83 Linköping
+46 13 28 10 00 , www.liu.se

Abstract

This thesis explores the potential of second-life electric vehicle batteries, which are no longer suitable for electro-mobility, to provide energy storage solutions. The study identifies two potential applications for second-life batteries: charging stations and residential PV energy storage systems. The research uses the remaining useful life as a vital indicator of the benefit that emerges from each solution. A battery aging framework is proposed, taking power demand and temperature as inputs and generating capacity loss and resistance increase utilizing aging models from the literature. It is observed that the prediction can vary significantly depending on the model. Additionally, the total costs of each solution are heavily influenced by the battery pack configuration, as EV batteries can be directly reused or refurbished. A lower degree of dis-aggregation and testing is more cost-effective and entails fewer wasted components, yet it introduces performance uncertainties. The study concludes that applications that can tolerate uncertainties and inflexibility are best suited to meet the supply of second-life EV batteries. Furthermore, by re-purposing second-life batteries, there is potential to maximize their value and reduce environmental impact by reducing the need for new batteries.

Acknowledgments

This study was only possible with the guidance and support of several people. First, I would like to thank Arne Erlandsson at Modular Management for always being willing to discuss various aspects of the work and share expertise and knowledge. Second, I want to thank Colin de Kwant for believing in my work and steering the project in the right direction. Your thoughts and ideas have opened my eyes to new fields and made the past six months a learning experience. Lastly, I want to thank Rikard Bodén, who has been persistently supportive and optimistic about the work.

Furthermore, I would like to thank Daniel Jung, my supervisor at Linköping University, for your feedback and guidance during our meetings. Your in-depth knowledge of vehicular systems and modeling has proven invaluable.

Elis Sandberg
Stockholm, 20230620

Contents

List of Figures

List of Tables

Nomenclature

Abbreviations

Abbreviation	Meaning
AC	Alternating Current
BESS	Battery Energy Storage System
BMS	Battery Management System
CS	Charging Station
DC	Direct Current
DOD	Depth of Discharge
EMS	Energy Management System
EV	Electric Vehicle
ESS	Energy Storage System
GHG	Greenhouse Gas
HEV	Hybrid Electric Vehicle
LFP	Lithium-Iron-Phosphate
MO	Metal Oxide
MPPT	Maximum Power Point Tracker
NCA	Nickel-Cobalt-Aluminium
NMC	Nickel-Manganese-Cobalt
PV	Photovoltaic
RUL	Remaining Useful Life
SEI	Solid Electrolyte Interface
SOC	State of Charge
SOH	State of Health

Symbols

Notation	Description	Unit
E	Stored energy	Wh
Q	Total capacity	Ah
R_0	Internal resistance	Ω
I	Current	A
U_{OC}	Open circuit voltage	V
T	Temperature	K
P	Power	W
R	Ideal gas constant	$J\text{mol}^{-1}K^{-1}$

1 Introduction

This chapter begins by introducing the subject of the thesis together with the background of the problem. The research purpose and question are then presented, followed by a discussion of the main limitations.

1.1 Background and Problem

In 2019, the transport industry was responsible for 8.7 gigatonnes of direct greenhouse gas (GHG) emissions, which made up 23% of global energy-related CO_2 emissions, according to IPCC's Sixth Assessment Report. Road vehicles contributed to the bulk of these emissions, accounting for 70% [1]. Transport-related emissions in developing countries have been increasing faster than in Europe and North America, and this trend is expected to continue in the following decades. Following this, decreasing global transport emissions of greenhouse gases will be challenging since the increase in passenger and freight activity may negate the efforts. Hence, improved technologies are needed to decouple transport emissions and economic growth significantly.

Electric vehicles EVs are becoming increasingly prevalent as a means of transportation. According to estimates from the International Energy Agency, the number of EVs on the roads is projected to reach 145 million by 2030 [2]. While the use phase of EVs does not produce carbon dioxide emissions, the environmental impact of EVs extends beyond this phase. It encompasses the entire value chain, from acquiring raw materials to end-of-life treatment. One of the critical components of an EV that contributes to its environmental footprint is the battery. EV batteries are material-intensive and contain toxic and heavy metals, which can have negative environmental consequences. Furthermore, when the battery reaches the end of its useful life, the environmental benefits of the EV are largely negated. Therefore, it is essential to prioritize the re-usage and recycling of EV batteries.

1.2 Research Purpose and Question

The International Energy Agency (IEA) reports over 16.5 million electric vehicles on the roads worldwide. Soon, many of these batteries will no longer be suitable for electromobility purposes, leading to the question of how they should be managed to retain maximal value. One option is to reuse the batteries in applications with lower demands on energy density, such as trucks and forklifts. Another option is to reuse the batteries in stationary applications where peak power and energy density, to a less extent constitute limiting factors.

When considering the installation of a degraded battery in a stationary application, the remaining useful life (RUL) becomes a critical factor, as it is closely related to the overall profitability. The RUL refers to the estimated number of years that a component can still perform its intended function before requiring replacement. If the battery is depleted rapidly, the investment may not be justifiable. This thesis aims to evaluate various second-life applications for EV batteries, utilizing the RUL as a key performance indicator. The assessment

is complemented by a cost analysis, which accounts for the acquisition and reconfiguration of EV batteries and other associated components. The two research questions are outlined below. The first research question is quantitative, while the second has a more qualitative approach. Combining these two research methods provides richer and more comprehensive insights.

RQ1: How does the RUL of second-life batteries differ in stationary applications?

RQ2: What are the primary technical and economic obstacles to implementing second-life batteries in stationary applications?

1.3 Research Setting and Scope

This research aims to outline the aging behavior of lithium-ion batteries to determine the RUL in different second-life applications and scenarios and asses the associated costs. However, the framework is not developed for battery research and design optimization. Thus it only captures the main degradation processes and disregards intricate chemical reactions and processes such as lithium plating and hysteresis effects. Furthermore, given the time constraint, only a limited number of applications and scenarios are studied. The process of creating the scenarios involves several assumptions and uncertainties. Sweden is used as a point of reference for any assumptions related to external circumstances such as grid infrastructure and weather conditions. Alternatively, the assumptions are on the conservative side.

1.4 Thesis Outline

This thesis does not rely on experimental testing to generate new data. Instead, a simulation framework is developed and coupled with input data to describe battery aging in stationary applications. Chapter 3 presents common premises for modeling the battery aging process. In addition, well-established models from the literature are reviewed and compared to lay the foundation for the aging framework. In chapter 4, the scenarios are introduced. The first scenario is a charging station coupled with a battery energy storage system (CS-BESS), and the second scenario is a residential PV system with a battery energy storage system (PV-BESS). Two applications are deemed appropriate due to time limitations. These particular applications are selected because they involve various configurations and have diverse operating voltages and power flows. Chapter 5 focuses on the cost of utilizing second-life batteries in stationary applications. This involves the cost of acquiring second-life EV batteries and the required modifications to make them suitable for stationary use. Various configurations and topologies are examined, along with the common trade-offs. The aim is to guide the decision-making process. Chapter 6 discusses the results and addresses some significant barriers to reusing EV batteries in stationary applications. The last chapter discusses to what extent the research objectives are achieved and the implications for the target audience. It also includes a modest proposal for future work on the same subject.

2 Theoretical Framework

The chapter starts with a short overview of the EV industry and current trends. A description of the working principles of a lithium-ion battery follows this. Then, within the same section, the EV battery system is outlined, which includes the most critical components. Last, EV batteries' recycling and reuse processes are explained, along with the presentation of various stationary battery applications.

2.1 Battery Electric Vehicles

The number of EVs has increased substantially in recent years. In 2021, it was estimated that approximately 10% of global automobile sales were composed of EVs, with a total global population of approximately 16.5 million. The acceleration in the development of EVs can be attributed to various factors, including an increasing number of countries committing to phasing out internal combustion engine vehicles and implementing ambitious plans for electrification. Furthermore, the International Energy Agency statistics indicate that public spending on subsidies and incentives for EVs nearly doubled in 2021 [2]. Additionally, the availability of EV models in the market has increased, with the number of models in 2021 being five times greater than in 2015. The transition to EVs is seen as a crucial step in decarbonizing road transportation, as the total emissions of greenhouse gases throughout the entire lifecycle of an EV are typically lower than those of an internal combustion engine vehicle [3].

The battery energy storage system is essential as EVs use electric motors for propulsion. In the early days of EVs, lead-acid batteries were commonly used, although they were heavy and had limited range. In the 1900s, nickel-metal hydride batteries were introduced, with higher energy density and improved range. Today, the most common choice among vehicle manufacturers is lithium-ion batteries due to their superior energy density, high efficiency, and good temperature performance. In the category of lithium-ion batteries, there exist various types of cathodes comprising different metal oxides, each of which has its own set of trade-offs concerning performance and cost. The chemistries most commonly used in electromobility applications are nickel cobalt aluminum (NCA), nickel manganese cobalt (NMC), and lithium iron phosphate (LFP). When comparing the energy densities of commercial single cells, NMC lithium batteries have an energy density of around 230-250 Wh/kg. In comparison, NCA batteries have an energy density of about 320 Wh/kg. In 2020, the energy density of LFP lithium batteries was around 130-160 Wh/kg [4].

2.2 Lithium-ion Batteries

Working Principles

The material in [4] explains the working principles of lithium-ion batteries. A lithium-ion battery comprises two electrodes, an electrolyte, and an outer circuit. The electrodes are denoted anode and cathode depending on the relative voltage potential. The electrolyte facil-

itates lithium-ion transportation from the cathode to the anode while inhibiting electron flow. By providing a separate pathway for the electrons, the current may pass through a power device before returning to its stable state, also referred to as charge balance. For safety reasons, an additional separator is incorporated between the electrodes. This separator, characterized by its micro-porosity, permits the passage of lithium-ions while impeding electron flow. The formula below illustrates the reversible reaction that occurs in lithium-ion cells.

$$Li_xC_6 + Li_{1-x}MO \rightleftharpoons C_6 + LiMO$$

Electrons do not come into contact with the electrolyte due to a phenomenon that occurs during the initial charge cycle of the battery. As lithium-ions traverse the electrolyte layer, solvent electrolyte molecules envelop the ions. These molecules subsequently react with the graphite (anode), creating a solid electrolyte interface (SEI). This layer serves to protect the electrolyte from electron exposure. Figure 2.1, obtained from [5], shows the parts of a lithium-ion cell. Much research has been dedicated to reducing the separator's thickness, which enables the electrodes to accommodate more lithium-ions, resulting in higher energy density [6]. However, this involves a compromise between battery safety and performance.

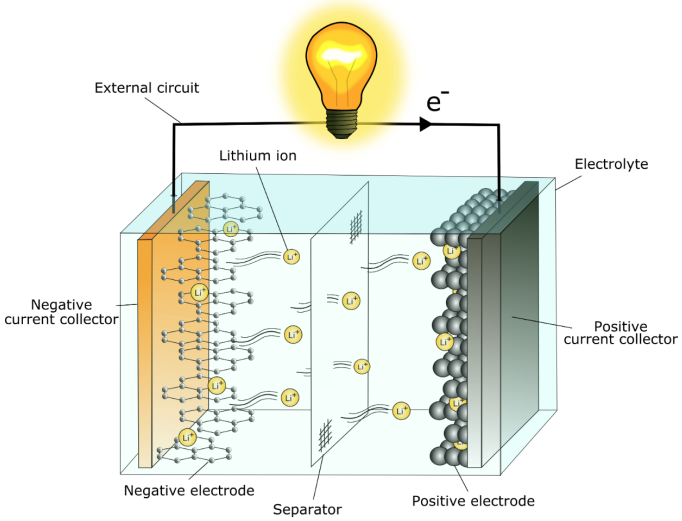

Figure 2.1: Schematic of a lithium-ion cell.

Lithium-ion Batteries in EVs

An EV battery pack typically comprises hundreds to thousands of cells connected in serial and parallel configurations. Connecting batteries in series and parallel impacts the output voltage and capacity of the system. These electrochemical cells operate within a voltage range of 2.5-4.2 volts. The voltage in a cell should not fall below two as the anode will start dissolving, forming copper passages/shunts, which accelerates self-discharge. Similarly, the cells can be damaged by overcharging as the cathode decomposes. The cells come in cylindrical, prismatic, or pouch sizes. Cylindrical cells are more cost-effective and have a relatively higher energy density, while prismatic cells are more compact but may be more expensive to produce [7]. Cells are grouped into modules to facilitate the manufacturing process, and multiple modules can be positioned within a metallic housing to form a battery pack. Figure 2.2 provides a visual representation of the critical components of a battery pack. The BMS is located inside the battery pack and uses the Controller Area Network (CAN) to communicate

with the main computing unit of the vehicle. However, to be able to decode the messages, a CAN matrix[1] is necessary.

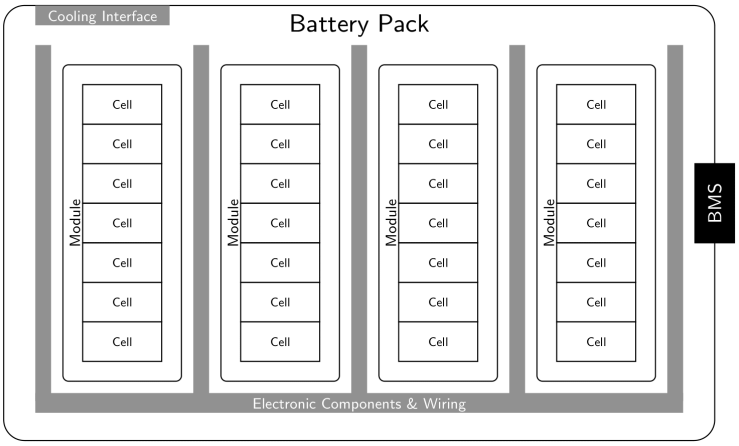

Figure 2.2: The figure illustrates a battery pack consisting of multiple cells and modules.

A BMS is an embedded system that ensures the battery's safe and optimal operation, acting as an interface between the battery and the main computing device. The BMS monitors and controls temperature, voltage protection, SOC, and SOH. The SOC is measured and estimated using several methods, e.g., coulomb counting, open circuit voltage, electromotive force, Kalman filter, and particle filter. With this, the BMS can equalize the voltages of individual cells to prevent over- and under-voltage [8]. Car manufacturers are generally reluctant to share details concerning the specific algorithms used in the BMS [9]. Active balancing is classified into three different categories, presented below.

- **Cell balancing based on capacitor:** Capacitors assist in achieving cell balance by transferring energy between adjacent cells. The main drawbacks include energy loss during capacitor charging and a delay in achieving balance.
- **Cell balancing based on a transformer:** Transformers or inductors can transfer energy between cell modules or cells to achieve cell balance. This facilitates rapid equalization of cell voltages. However, one drawback of this approach is the requirement for filter capacitors at each cell.
- **Cell balancing based on converter:** Effective cell balancing can be achieved with DC-DC converter such as buck, boost and flyback. However, high cost and complexity remain essential issues [8].

[1]The CAN matrix is a table structure that defines the communication relationships between the vehicle control units in a CAN bus network. It specifies which units can send and receive messages and their unique identifiers and permissions. The matrix helps manage data flow, prioritize messages, and communicate properly.

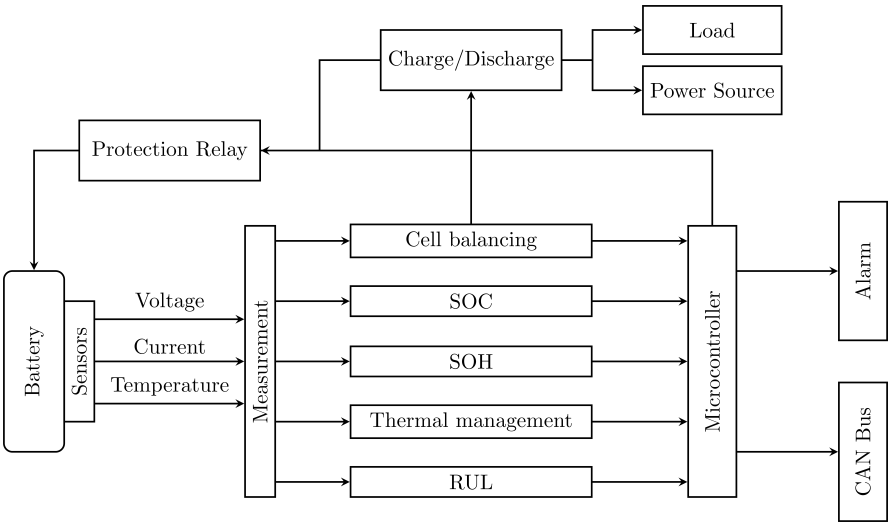

Figure 2.3: Battery Management System adopted from [8].

Another critical system in an EV battery pack is the cooling system. High temperatures accelerate the aging of batteries. Therefore, thermal management is a major concern for EV manufacturers. Air and liquid cooling are two options to combat heat accumulation in the battery. These systems typically involve external devices such as fans, pumps, heat sinks, and cooling fluids. Liquid cooling systems have many specialized designs, from simple cooling plates under the batteries to in-between cell cooling channels [10].

2.3 Reusing EV Batteries

A circular economy is usually defined as an economic system based on reusing and regenerating materials and products. Much research has been done on efficiently recycling batteries to extract the different materials [11],[12]. Stockpiling or landfilling is generally undesirable as the materials would be wasted, and the significant investments and work effort in the production phase would not be well used. However, recycling batteries is a complex process with numerous technical and logistical challenges. A study by Kotak et al concludes that the recycling mass efficiency, expressed as the ratio between the mass of the output fractions and the mass of the input fractions, is around 50% for lithium-ion batteries, which is significantly lower than for lead-acid batteries and nickel-cadmium batteries [3]. In addition, not every metal can be recycled at a reasonable price. An example of this is lithium which typically constitutes 2-7% of the weight of a lithium-ion battery. However, obtaining this material through recycling is five times more expensive than obtaining it from natural resources [13]. In the context of lithium-ion batteries, the only profitable material to recycle is cobalt, as it is the most economically valuable material. As a result, the benefit largely depends on the metal concentration [14], with decreasing concentrations of cobalt, the economic benefit vanishes. Figure 2.4 illustrates a flow chart of how degraded EV batteries can be treated.

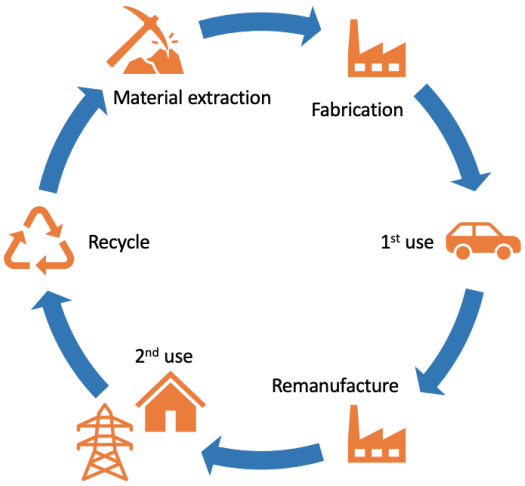

Figure 2.4: A circular economy framework for EV batteries.

Reusing batteries is the most cost-efficient and sustainable option as the battery's lifespan is extended, and activities such as dismantling, smelting, and refining are postponed. Degraded batteries can be implemented in many applications, from energy storage systems to industrial applications. There are two main approaches to reusing EV batteries. The first strategy involves maintaining the battery pack as a single entity and only conducting visual inspections and electrical tests. The second strategy involves dismantling the battery into modules or cells, testing them individually, and then grouping them to form a new battery that meets the specific requirements of the second-life application. The former approach refers to direct reuse, while the latter is refurbishing [15].

Testing and reconfiguring the battery pack are necessary to implement a second-life EV battery into stationary applications. However, the extent of these procedures depends on specific requirements and customer preferences. Since batteries can be composed in various ways, the design of the new battery storage system is crucial. To address this issue, Montes et al. [16] proposed a framework for determining possible configurations of second-life batteries for different stationary applications. Generally, higher-demanding applications require multiple reused battery packs, whereas lower-demanding applications may demand dismantling battery packs into modules and cells. A higher level of dis-aggregation allows the end user to tailor the system to suit the specific purpose. Nevertheless, this entails a higher cost and more wasted components. Each configuration has its advantages and disadvantages. The following section discusses these in more detail.

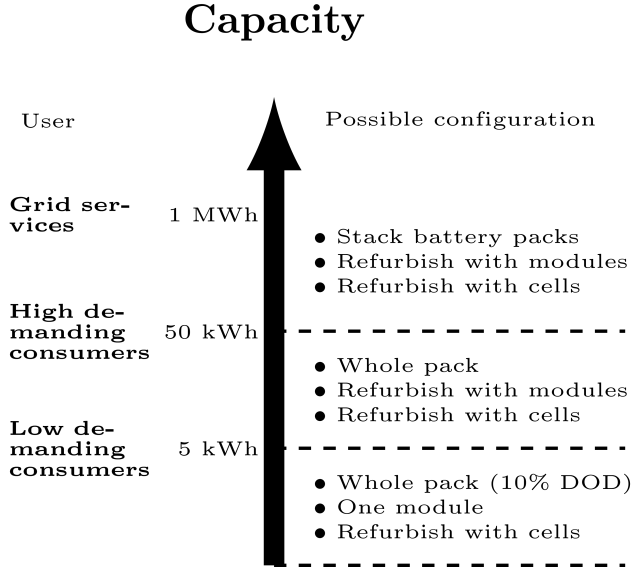

Figure 2.5: The figure shows the possible configurations for different stationary applications. Adopted from [16].

In the paper "End of Electric Vehicle Batteries: Reuse vs. Recycle" Kotak et al. indicate that reusing batteries in stationary applications has clear benefits but mentions that it involves high costs of life cycle assessment. An optimal solution cannot be provided for all cases, and a detailed study of each application is called for [3]. Sharing critical information along the value chain is a major obstacle to reusing EV batteries. Obtaining information such as the cathode material, usage history, and battery condition is crucial but often challenging. This, in turn, requires the BMS to accurately monitor the SOC and SOH to predict the battery's usability [17]. Additionally, the transportation of the batteries after they are removed from the vehicle is restricted due to hazardous waste regulations, making logistics and transportation a costly and challenging part of the process. Another obstacle is the need for more standardization, which makes it difficult to swap batteries between different applications and establish a sufficiently liquid trading place [18].

2.4 Stationary Energy Storage Systems

Battery energy storage systems have a wide range of applications, varying in scale from small residential units to containerized solutions in the distribution system. Additionally, the duration of the storage can vary from short-term to long-term or seasonal, depending on the user requirements [19]. At the time of this study, commercial battery energy storage systems have yet to be widely established [13]. However, test projects have been launched, indicating that the research field is just beginning to form. Nonetheless, the expansion of stationary battery storage depends on its ability to provide value to the end customers. Typically, battery energy storage systems are classified as either behind the meter or in front of the meter, depending on their position relative to the electrical measurement device. A behind the meter battery is located on the customer's property and not integrated into the electricity grid. Conversely, an in front of the meter battery is integrated into the grid. Figure 2.6 illustrates how degraded EV batteries may be used in second-life applications as the SOH declines.

In Front of the Meter

In front of the meter batteries typically provide grid and utility-scale services where they play a significant role in integrating renewable energy sources and storing excess energy. More specifically, the batteries can be used for frequency and voltage control, peak-shaving, congestion management, and black start services [20]. This contributes to securing the stability of the electricity system, as slight deviations from the standard can cause damage to connected appliances and equipment. In summary, stationary batteries can be repurposed for use in grid infrastructure to make the grid more cost-effective, reliable, resilient, and safe. This can be done at the distribution or transmission level [21].

Behind the Meter

Behind the meter applications usually involve commercial, industrial, and residential establishments. In these applications, the stationary battery can enable the maximum self-consumption of renewable energy, smooth integration of EV charging stations with the grid and provide other auxiliary services. The main benefit is related to the reduction of investments cost and revenue streams to the end user while additionally providing balancing services to the grid. These benefits are particularly relevant as the adoption of renewable energy sources, and EVs continues to grow, and the grid requires more flexibility to manage the variability of renewable energy sources.

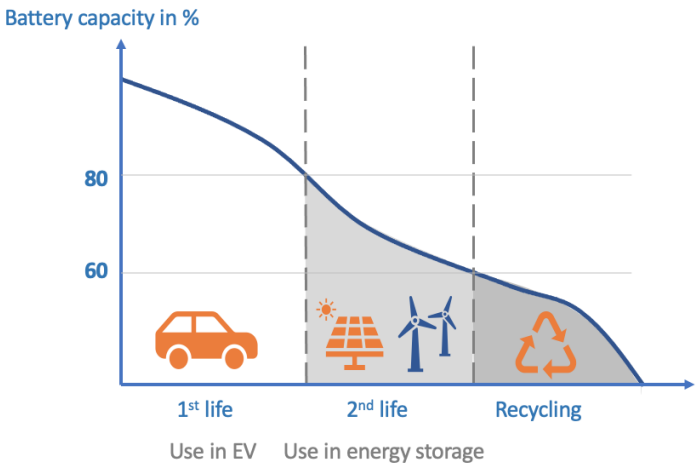

Figure 2.6: The figure illustrates how battery packs can be re-purposed in different applications as the SOH declines.

2.5 Battery Metrics

This section presents some important parameters related to battery technology and the aging process.

Energy density: The amount of energy that a battery is carrying per weight unit. Often presented as Wh/kg.

Power density: The amount of power that can be delivered per weight unit. Often presented as W/kg.

State of charge (SOC): State of charge describes the energy in a battery that can be extracted by discharging it to the cut off voltage limit. The extractable energy at one point in time is divided by the energy at the fully charged state, which yields a percentage ranging between 0% and 100%.

$$SOC = \frac{Q}{Q_0}$$

where Q is the remaining capacity of the battery and Q_0 is the fully charged capacity.

State of health (SOH): State of health describes the available amount of energy that one can extract before the battery stops operating correctly or breaks down.

$$SOH = \frac{Q}{Q_{nom}}$$

where Q is the current maximal discharge capacity and Q_{nom} is the nominal discharge capacity.

Depth of discharge: Depth of discharge describes to which extent a battery is discharged during one cycle. It is calculated by subtracting the remaining capacity of the battery from its maximum capacity and then dividing the result by the maximum capacity. High depth of discharge means that more charge is extracted during a discharge cycle.

Self-discharge rate: Self-discharge rate refers to the rate at which a battery loses its charge when it is not in use or when it is disconnected from a circuit. A lithium-ion battery typically self-discharges at a rate of about 5% per month, depending on the type and temperature of the battery.

C-rate: The C-rate is defined as the rate at which a battery is charged/discharged. If a battery has a capacity of 1 Ah and a C-rate of 1, it means that the current is 1 Ampere during discharge. In lithium-ion batteries the C-rate typically varies between 0.5C (energy cells) and 5C (power cells), although higher C-rates of up to 25 are allowed in short pulses. In battery energy storage systems the C-rate is usually below 1 [16].

End-of-life End-of-life refers to the point at which a battery is no longer able to perform its intended use. SOH and internal resistance are two metrics commonly used to determine when this is the case. E.g., when an EV battery reaches 80% SOH or when the internal resistance has increased with 100%. The relative capacity threshold is usually linked to high energy EV applications while the internal resistance threshold is linked to high power EV applications [16].

3 Method

The chapter starts by providing an overview of the modeling methods utilized for lithium-ion batteries. Subsequently, it explores the degradation of batteries and the various modeling approaches employed. Additionally, the chapter includes a critical evaluation of lithium-ion aging models found in various literature sources. The final part of this chapter outlines the overall approach used for estimating the RUL of batteries in stationary applications and the cost estimation process. The last section connects the battery aging framework with the subsequent chapters.

3.1 Modeling Battery Characteristics

Alongside the evolution of new battery technologies, new models have been developed for describing battery characteristics. A model is used to approximate the response of a system to different inputs, which can facilitate the prediction and optimization of basic parameters. The approaches can generally be divided into black box, electrochemical, and equivalent circuit modeling. Black box modeling involves conducting experiments to observe and measure the system's behavior [22]. For example, neural networks can be used to describe the relationship between input and output [23]. The disadvantage of black box modeling is that the model performance is highly sensitive to the quality of the training data [24]. The electrochemical model derives its mechanisms from the reactions inside the battery to establish a partial differential equation of the electrode and electrolyte kinetics. It is generally very accurate and complex, often desirable in battery research.

The equivalent circuit model (ECM) is used to simulate the physical macroscopical quantities of a battery cell. The ECM describes the electrochemical system as a simple electric circuit with circuit elements such as capacitors, resistors, and constant voltage sources. The benefit of this model is that it can be expanded upon to capture more detailed dynamics while still being relatively accurate and computationally efficient. Moreover, the parameters may be adjusted to account for varying external conditions such as temperature by adjusting the circuit parameters accordingly [25],[26].

Different ECMs exist that capture the dynamic voltage response of a battery. The most common types are the internal resistance, resistance-capacitance, and Thevenin model. The main difference is the number of components and the configuration. The internal resistance model consists of an internal resistance and open circuit voltage, capturing the power exchange but leaving out the transient behavior during charge and discharge operations. The model is often considered simple and has few applications in battery research and design optimization [22]. However, in this work, the internal resistance model is considered sufficient to describe the power exchange between a battery and a load. Figure 3.1 shows ECM employed. U_{oc} is the terminal voltage, which can be considered an ideal voltage source. R_0 is the internal resistance, characterizing the efficiency of the battery, including ohmic resistance and the charge transfer resistance. U_L is the load voltage.

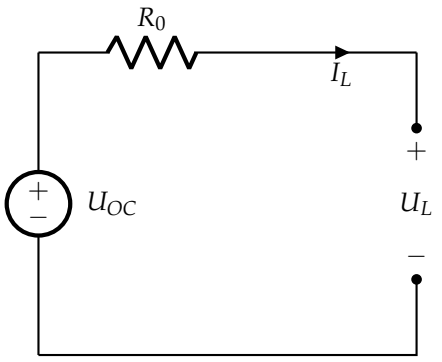

Figure 3.1: The figure illustrates a simple internal resistance ECM.

3.2 Modeling Battery Degradation

Lithium-ion batteries are complex electrochemical systems that undergo degradation due to various processes and interactions. The driving mechanisms behind battery aging have been outlined in previous studies [27],[28]. It is stated that the primary contributor to the degradation of lithium-ion batteries is changes at the electrode/electrolyte interface as a consequence of parasitic reactions such as SEI formation and other decomposition reactions. As stated in chapter 2, the SEI layer at the anode forms during the initial charging cycles. However, long term, it continues to become thicker as the SEI penetrates into pores of the electrode. This process is exacerbated by low potentials on the graphite side, which occur during battery charging. Similarly, elevated temperatures cause the SEI layer to break down, requiring a new one to be formed, which allocates lithium-ions to the SEI layer and reduces capacity. [27]. Another reaction that reduces the lithium inventory is denoted loss of active material. This can be due to particle cracking and loss of electrical contact or blocking of active sites by restive surface layers [29]. Capacity loss data of a common lithium-ion battery is presented in Appendix F and G.

Numerous models have been developed to describe the aging process of lithium-ion batteries. Most of which focus on automotive applications such as HEVs. One of the most cited studies is authored by Schmelstieg et al. The authors studied the aging of NMC lithium-ion batteries, examining both calendar and cyclic aging. The study considered various stress factors such as temperature, SOC, and DOD. With a semi-empirical approach, the Arrhenius law parameters (activation energy and the pre-exponential constant) are determined to understand the impact of temperature [30]. However, it is important to note that only a single current magnitude was used in the study.

In a separate study, Wang et al. explored battery aging by examining different DOD levels, temperatures, and current rates. One clear weakness of the study is that the authors did not conduct designated tests to determine the impact of calendar aging. Instead, the cyclic aging tests with low C-rates were accepted as an indicator of calendar aging [31]. This is a strong assumption as a significant amount of charge throughput impacts the aging process. Moreover, the authors did not consider SOC as a factor influencing aging. A study that incorporates SOC but leaves out the C-rate as a stress factor was conducted by Smith et al. The model is developed to describe the aging of NCA lithium-ion batteries used in HEV applications. The study focuses on vehicular applications and proposes several actions to mitigate battery aging. For example, the authors suggest oversizing the battery to avoid reaching 100% SOC, even though this would result in higher costs [32].

A study focusing on battery aging in stationary applications was conducted by Xu et al.

The authors propose a semi-empirical model to describe battery degradation resulting from irregular operations. Their model considered factors such as DOD, SOC, and temperature. The model is used to simulate various batteries' degradation processes in frequency regulation applications. With a broad set of test data, it was observed that batteries exhibited significant differences, even batteries of the same type [33]. Finally, a study of lithium-ion battery aging with LiFePe batteries was conducted by Neumann et al. Only exploring calendar aging, the test was running over a total duration of 29 months. According to their findings, the battery's calendar life could reach 22 years before the SOH drops below 80%.

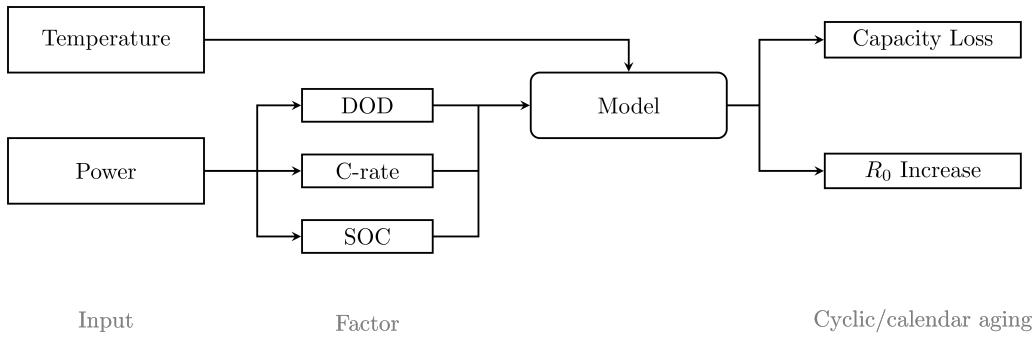

Figure 3.2: The figure illustrates the aging framework. Temp, SOC, C-rate and DOD constitutes the stress factors.

In view of the aforementioned studies a battery aging framework is developed in this study. The framework, depicted in Figure 3.2, aims to capture the most common stress factors. The power profile and temperature serve as inputs to the model. The stress factors are deducted from the inputs mentioned above. Battery aging is characterized as a change in capacity and internal resistance, as these together quantify the stored energy and power of the battery cell. The simulations are performed at cell level. To obtain representative results for an entire battery pack, it is assumed that the aging process is uniformly distributed and that the battery pack is equipped with a sophisticated BMS. This is further discussed in section 4.4.

3.3 Second-stage Degradation and Path Dependency

Lithium-ion batteries can exhibit linear, sublinear, or superlinear aging. Sublinear aging is often attributed to side reactions such as SEI growth, which grows approximately with the square root of time or charge throughput due to its self-passivizing nature [34]. As the aging rate decreases, this behavior is highly desirable for long-life applications. However, superlinear aging is also commonly observed, where the SOH suddenly drops off, which also may entail a collapse in safety. This type of nonlinear degradation has many names, such as "second-stage degradation," "aging knee," and "drop-off." Delaying second-stage degradation is of great importance for extending the battery lifetime. Also, the unpredictable nature of the phenomena makes RUL estimation challenging, as batteries with the same SOH can have vastly different RULs. Previous literature has identified failure modes that lead to second-stage degradation. This includes lithium plating, electrode saturation, resistance growth, and mechanical deformation [34]. Predicting the onset of this has been performed with neural-networks in [35]. This work conservatively assumes that the capacity restricts the battery life and that the aging models are valid until the battery reaches the lower bound SOH of 70%.

When empirically developing battery aging models, experimental data is usually generated in constant storage or cycling conditions [36], but in most applications, these conditions are not constant. Path dependency refers to the phenomenon where historical charging and

discharging patterns influence the performance and characteristics of a battery. Accounting for path dependency makes the test procedure significantly more resource-demanding as dynamic cyclic aging tests must be applied with changing SOC, DOD, temperature, and discharge rates. However, previous studies have concluded that path dependency is most significant for lithium-ion batteries for high C-rates [37]. In light of the above, this work assumes that the capacity fade and resistance increase behaves path-independently.

3.4 Selected Models

Since few to no battery aging models are available that have been developed explicitly for second-life applications, models developed for other applications have been used. This work selects three models to serve as governing equations in the simulations to obtain a balanced perception of the degradation process. All models have been developed with semi-empirical methods, which is usually advocated as it allows plenty of new insights to be gained at a reasonable price. The particular models have been selected based on a few criteria, applicability to multiple aging scenarios, and overall soundness. It is also considered advantageous if the calendar and cyclic aging are modeled separately, as the batteries in the scenarios in this study involve batteries that are in idle mode for significant time durations.

Table 3.1 presents the different models and associated properties. Although all models are developed for NMC lithium-ion batteries, model number three is established on a battery with a blended cathode. Moreover, the models include unique sets of stress factors. By studying the research papers [38], [30] and [39], it is noticeable that the underlying assumptions lack consistency. Thus, one must remember that the models are contingent on the intended purpose and application and should only be compared with scrutiny. Another remark is that two models were designed to accommodate HEV usage scenarios. For each model, the numerical parameters are presented in Appendix A-C.

Table 3.1: Aging models and properties.

Model no.	Author	Chemistry	Stress factors
1	Baghdadi	NMC	T, SOC, I
2	Cordoba	NMC-LMO	T, SOC, ratio
3	Schmalsteig	NMC	T, SOC, DOD

Model 1

The model presented in [38] is considered one of the most comprehensive and accepted in literature. The model includes calendar and cyclic aging with respect to capacity and power fade and incorporates the most important stress factors. Moreover, the model has been calibrated with a broad set of experimental data to fit different lithium-ion battery types and chemistries.

The parameters used in this work have been calibrated to represent the aging process of an NMC lithium-ion battery cell. The model features temperature, SOC, and current as stress factors. The calendar aging data is generated from nine experiments with temperatures ranging from 30°C to 60°C and SOC levels between 30% and 100%. The power cycling experiments are constructed to emulate a HEV charge and discharge profile. Therefore, the charges and discharges occur as short pulses with high C-rates. The calibrated model parameters a_1 to a_6 are reported in Appendix A.

The developed model has a chemical rate approach, where the total degradation is expressed as an exponentially decaying function of the time multiplied by the degradation rate. The calendar aging rate is expressed with temperature and SOC as variables, i.e., the thermo-oxidative aging factors. The cyclic aging factor is calculated and multiplied with the calendar aging factor to determine the total aging factor. Thus, charging and discharging operations amplify the calendar aging. The exponential functions governing the change of capacity Q and internal resistance are provided in equation 3.1 and 3.2.

$$Q_{loss,\%} = \exp(-k_{tot} t^n) \tag{3.1}$$

$$R0_{inc,\%} = \exp(k_{tot} t^n) \tag{3.2}$$

Q and $R0$ represent the capacity and internal resistance at time instant t. k_{tot} is the total aging factor equal to the product of the cyclic aging factor and the calendar aging factor. The reaction order n is set to 1.

$$k_{tot} = k_{cyc} \cdot k_{cal} \tag{3.3}$$

k_{cal} is expressed as the integral of the calendar aging rate with respect to SOC.

$$k_{cal,avg} = \frac{1}{\Delta SOC} \int_{SOC_{min}}^{SOC_{max}} \exp(\frac{a_2 SOC}{a_1}) \cdot \exp(\frac{a_3}{a_1}) \cdot \exp(-\frac{a_4}{a_1 T}) \mathrm{dSOC} \tag{3.4}$$

The cyclic aging rate k_{cyc} is a function of the applied current I and temperature T. R is the ideal gas constant.

$$\ln(k_{cyc}) = \exp(\frac{a_5}{RT} + a_6) \cdot I \tag{3.5}$$

The total degradation rate is the product of the calendar and cyclic degradation rates. Figure 3.3 illustrates the results from simulated calendar aging processes. The different lines represent combinations of temperature and SOC. Elevated temperatures and high SOC levels accelerate the aging process. However, for temperatures of 20°C the capacity loss is below 12% in the first two years. Similarly, in advantageous temperature conditions, the resistance increase is below 30% in the first two years.

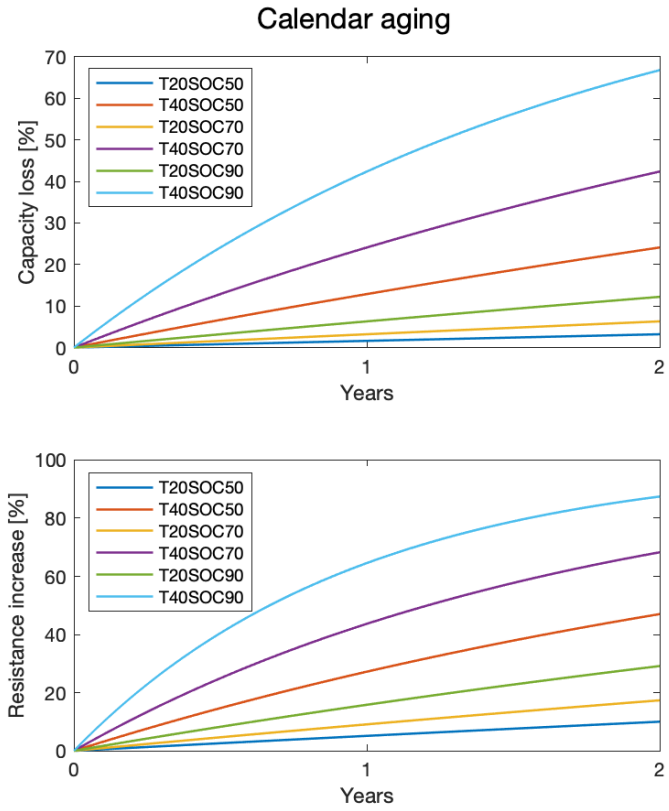

Figure 3.3: The figure illustrates the calendar aging of a battery according to model 1.

Model 2

The model proposed by Cordoba et al. [39] is designed to assess batteries' SOH and provide an EOL prognosis. The study focuses on lithium-ion batteries containing NMC-LMO metal oxides. Various experiments were conducted under different C-rates and a lower bound on SOC at temperatures ranging from 10°C to 45°C.

In this model, the capacity loss is determined using the Arrhenius equation and a severity factor. The severity factor depends on the ratio and minimum SOC reached during a cycle, denoted as SOC_{min}. The ratio is defined the proportion of time spent in charge depleting mode compared to charge sustaining mode. A higher ratio indicates a relatively longer duration of discharging. The activation energies for capacity and resistance, denoted as E_C and E_R, are considered along with the ideal gas constant R. The calibrated model parameters a, b and z are reported in Appendix B.

$$Q_{loss,\%} = a(SOC_{min}, ratio) \cdot \exp(\frac{-E_C}{RT}) \cdot Ah^z \tag{3.6}$$

$$a = a_1 + a_2 \cdot (ratio)^{a_3} \cdot a_4(SOC_{min} - a_5)^{a_6} \tag{3.7}$$

The resistance increase is also expressed using the Arrhenius equation. However, the resistance increases linearly with time, and the severity factor b is not a function of the charge rate CR.

$$R0_{inc,\%} = b(SOC_{min}) \cdot \exp(\frac{-E_R}{RT}) \cdot Ah \tag{3.8}$$

$$b = b_1 + b_2(SOC_{min} - b_3)^{b_4} + b_5 \cdot \exp[b_6(CR_0 - CR) + b_7(SOC_{min} - b_8)] \tag{3.9}$$

Since the calendar aging and cyclic aging are not modeled individually, the calendar aging process can not be visualised with this model.

Model 3

The aging model presented in [30] is established based on test data for an NMC lithium-ion battery. The specific battery type is commercially available, and consequently, a lot of public data is available.

The model includes calendar and cyclic aging to determine capacity and power fade. The two terms are added. The author proposes models with linear and non-linear time and charge throughput dependencies. The average SOC and temperature decide the calendar aging. Lower SOC decelerates the aging process. However, it is deducted that 3.7 is the optimal cell voltage, corresponding to approximately 40% SOC. The influence of depth of discharge is covered by including a linear dependency on DOD. The calibrated model parameters a_1 to a_7, b_1 to b_7, z_1 and z_2 are reported in Appendix C.

$$Q_{\%loss,cal} = (a_1 V_{avg} + a_2) \cdot \exp(\frac{-a_3}{RT}) t^{z_1} \tag{3.10}$$

$$Q_{\%loss,cyc} = [a_4 + a_5(V_{avg} + a_6)^2 + a_7 \cdot DOD] \cdot Ah^{z_2} \tag{3.11}$$

The resistance increase is expressed similarly. However, the optimal SOC are different.

$$R0_{\%inc,cal} = (b_1 V_{avg} + b_2) \cdot \exp(\frac{-b_3}{RT}) t^{z_1} \tag{3.12}$$

$$R0_{\%inc,cyc} = [b_4 + (b_5 V_{avg} + b_6)^2 + b_7 \cdot DOD \cdot Ah^{z_2} \tag{3.13}$$

Figure 3.4 illustrates the results from a simulated calendar aging process. Elevated temperatures and high SOC levels accelerates the aging. For temperatures of 20°C the capacity loss is below 5% in the first two years. The resistance increases less than 10% in the same period.

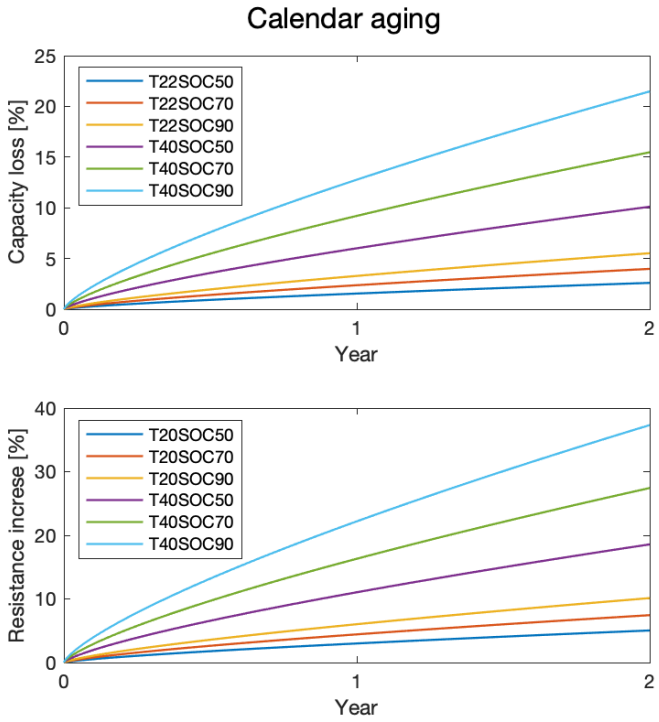

Figure 3.4: The figure illustrates the calendar aging for a battery according to model 3.

4 Simulation

This chapter starts by introducing the stationary applications that are studied in more detail. Then, different ad hoc methods are employed to decide appropriate battery sizes. Finally, the aging process of the batteries in the stationary applications is simulated, resulting in RUL estimates that serve as inputs for the cost analysis.

4.1 Stationary Applications

The current thesis examines how second-life batteries age under different stationary applications by simulating real-life scenarios to gain in-depth insights. One key assumption is that the batteries will be employed differently in each stationary application, including differences in charging and discharging characteristics and frequency of usage. For instance, the batteries may be used continuously, daily, or seasonally. Additionally, the batteries may operate under different external conditions. These parameters are listed in the table below for easy reference.

Table 4.1: Comparison of stress factors in different stationary applications

Application	Initial SOH (%)	Average SOC (%)	DOD (%)	C-rate
Residential PV-BESS	80	50	60	Low
CS-BESS	80	90	90	Medium

It should be emphasized that the parameters outlined in table 4.1 are not fixed, but rather determined by the size and condition of the battery and the power requirements. For instance, a battery that is larger than needed will result in a shallower DOD. The parameters can be determined using comprehensive optimization methods considering the costs of all components, depreciations, and storage. It is assumed that the initial SOH of the batteries is 80%. The average SOC and DOD levels are motivated in the following section. In the table above the C-rates are labeled using ordinal scale data. In stationary applications the C-rates are typically low [16]. However, due to the power requirements on the CS-BESS, the C-rate is slightly higher.

The figure in Appendix E shows the model used to simulate the aging process. The model consists of subsystems necessary to calculate the basic parameters and generate the aging output. The simulation is performed in the discrete domain, with sample times representing one hour. However, the parameters SOC, DOD, and C-rate are sampled once per 24 hours to obtain aging factors for each day.

4.2 Charging Station Battery Energy Storage System

Depending on the power level, an EV charging point typically outputs between 50 kW and 300 kW [40]. The prospect of implementing stationary batteries in EV charging stations has been studied in [41] and [42]. The economic advantage is that the grid does not have to

be expanded. However, the exact profitability depends on many factors such as the cost of the battery energy storage system, installation and maintenance and the charging demand and patterns of the station. Using an energy buffer to relieve the grid of power demand is commonly referred to as load shifting.

Scenario

Assuming that the CS-BESS is situated near a highway, the charging requirement during nighttime is insignificant. However, a considerable surge arises multiple times per week, which cannot be satisfied solely by the power from the grid connection. Therefore, to enable the integration of additional charging points, a stationary battery is utilized. The grid connection is limited to 500 kW. The stationary battery is discharged when the power demand exceeds 500 kW. As the circumstances demand quick charging times the charging station delivers DC power at with level 3 charging. With this the fees can usually be set comparatively high at 5-6 SEK/kWh to cover the expenses [43]. During periods of low occupancy, such as at night, the battery is recharged at 20 kW. The data underlying the power demand was obtained using a Google Maps API. It represents the relative customer influx for a petroleum station near a major highway in Sweden, which is considered a proxy measurement for the charging demand. While this data only constitutes an example of how the power demand can appear during a weak, for more reliable results, a stochastic approach needs to be taken regarding the arrival and departure of customers.

Battery Dimension

The stationary battery should be able to produce the difference between the peak demand and grid power supply. Considering the power demand in the scenario above it is clear that the highest demand is around 600 kW. However, the sum of the differences adds up to around 400 kWh during the days with the highest power demand. This is calculated according to the formula below. In equation 4.1 the difference between the power demand during peak hours $E_{EV,peak}$ and the grid power supply E_{grid} is used to calculate the total difference E_{diff}.

$$E_{diff} = E_{EV,peak} - E_{grid} \tag{4.1}$$

Furthermore, the DOD needs to be accounted for. Here 90% DOD is considered enough not to cause unnecessary harm when charging and discharging the battery. In equation 4.2 the nominal battery capacity E_{nom} is calculated.

$$E_{nom} = \frac{E_{diff}}{DOD} \tag{4.2}$$

Thus, the nominal battery capacity is 445 kWh. However, it is important to remember that the battery cells have a SOH of 80% in the beginning and are taken out of operation when reaching 70% SOH. A SOH decline of 12.5% takes place during operation, which also needs to be accounted for when sizing the battery system. The initial capacity is calculated in equation 4.3, c_{degr} is set to 87.5%.

$$E_{in} = \frac{E_{nom}}{c_{degr}} \tag{4.3}$$

The initial capacity of the battery is around 510 kWh. However, capacity is only one design parameter. One also has to consider the C-rate as a restricting factor. Many batteries have recommended limits on the C-rates not to damage the cell and create excess heat. Here it is assumed that the cells are of type 21700, presented in Appendix D. With a rated capacity of

4.8 Ah and a maximal C-rate of 2, it ultimately means that the output power can be at most 1,000 kW. This will not be the case as only four charging points are accommodated by the stationary battery.

Figure 4.1 shows the power demand during a week, as stated in the previous section. The grid connection of 500 kW is exceeded multiple times per week with a maximum power demand of 600 kW. With a battery size of 510 kWh, the battery is partially discharged multiple times a week. However, the DOD is not always the same, which must be considered in the simulations.

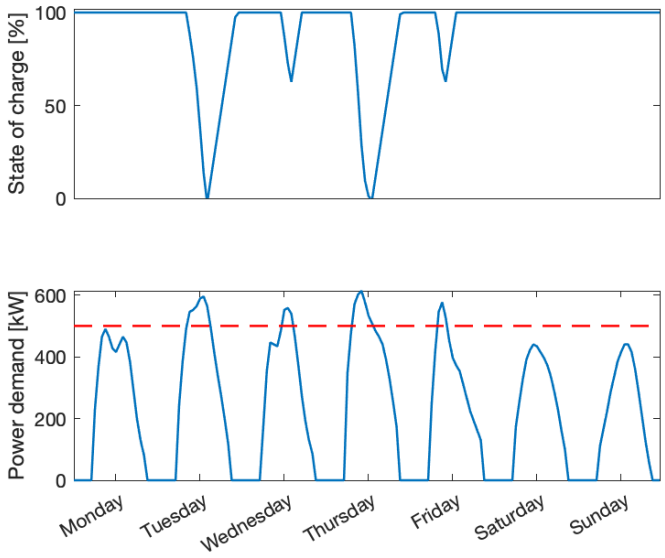

Figure 4.1: The figure illustrates the power demand in a charging station located by the highway during a typical week.

Given that the battery consists of lithium-ion 21700 cells with a rated capacity of 4.8 Ah and a nominal voltage of 3.7 Volts, each battery stores 17.76 kWh at the start. If the battery has an initial SOH of 80%, it must consist of more cells to provide the same power as a new battery. Taking this into account, the second-life battery will comprise 32,000 cells, weighing approximately 2 tons.

Simulation

The figure below illustrates the capacity decrease for a CS-BESS simulated with the models presented in section 3.4. The SOH is conservatively set to range between 80% and 70% as described in section 3.3, although this can change if new information is obtained about the battery characteristics and second-stage degradation.

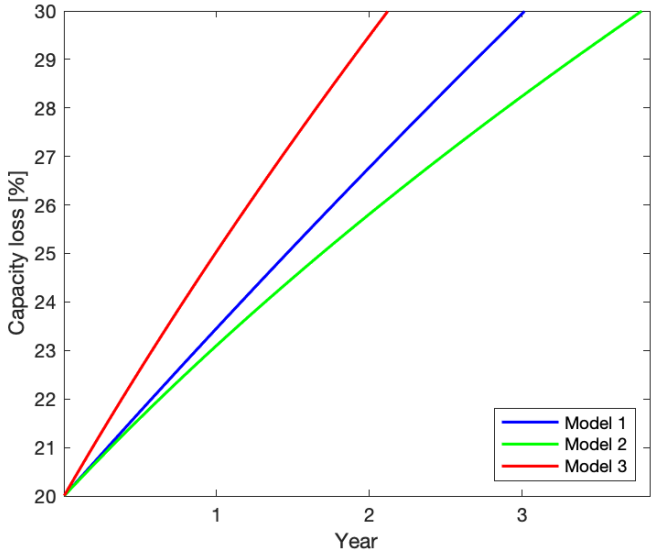

Figure 4.2: The figure illustrates the capacity loss for stationary batteries in a charging station.

Figure 4.2 shows the capacity decrease for a CS-BESS. The battery is assumed to be charged and discharged four times a week. The discharging is carried out at a maximal C-rate of 2 while the charging comparatively slow. Although, the charging and discharging modes can not be distinguished between in the simulation. The figure shows that the battery will reach 70% of the initial SOH within 2-4 years of continuous operation. However, there is a low degree of agreement between the models.

Apart from the capacity loss, the internal impedance increases with 22%. For a lithium-ion 21700 battery this corresponds to a final resistance of 244 mΩ. Furthermore, as the application is relatively high-power, a significant amount of heat is dissipated during operation.

4.3 Residential Photovoltaic Battery Energy Storage System

Residential establishments equipped with a PV-BESS can store energy when the production exceeds domestic consumption. This is advantageous because the excess energy does not have to be disposed of but can instead be consumed later. There exist different configurations for PV-BESSs. The systems may be AC or DC coupled. In AC-coupled systems, the PV generator is connected to an inverter that interconnects the grid, load, and battery on the secondary side. A charge regulator and inverter are placed between the AC side and the battery. DC-coupled systems have PV generators connected to the battery unit on the primary side of the inverter, while the secondary side connects the grid and load. The different configurations decide the overall efficiency and cost of the system [44]. When modeling a PV battery system, information such as the angle, temperature dependence, and degradation should be considered. A typical PV system battery operates at 24 or 48 V.

Scenario

Residential use of PV-BESSs can vary greatly. However, consumption data is based on data that represents the electricity consumption of suburban area in Sweden to design a realistic scenario. The data was collected from January to December 2020. The data has been averaged among 25 houses to represent a typical load profile and eliminate abnormalities. The average

yearly energy consumption is 9,500 kWh. As the houses are connected to a district heating system, the electricity consumption does not vary significantly with the season. Figure 4.3 illustrates the energy consumption during the day. The mean daily energy consumption is 26 kWh. Regarding solar production, global radiation data has been collected from SMHI for the same period as the consumption data.

It is assumed that the solar panels cover an area of 45 square meters and have an efficiency of 20%. Furthermore, the PV-cells are assumed to face south, whereas the temperature dependence is neglected.

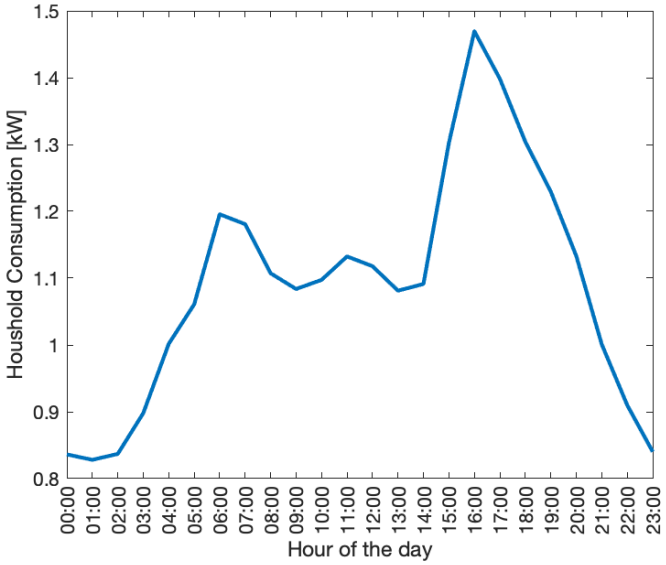

Figure 4.3: The figure illustrates the energy demand in a house during a day.

Stationary batteries in residential applications typically operate at a voltage level of 24 or 48 V. This is suitable for many EV battery modules.

Battery Dimension

Several studies have embarked on selecting optimal energy storage configurations for residential PV-BESSs [45]. It is generally agreed upon that the battery size has to be chosen in relation to the nominal PV power as well as the electricity demand of the household. A typical starting point when sizing stationary batteries is to consider the average demand between sunset and sunrise. Thus, one can ensure the battery does not carry residual capacity when the photovoltaic production starts. Using this heuristic, the size of the battery should be around 10 to 15 kWh.

Also, the specific needs of the user influence the issue of battery sizing. For example, while financial benefits may not be the sole aim, the customer might prioritize achieving greater self-sufficiency and resilience to power outages. However, this is less common in countries where the electricity supply has historically been reliant. The self-consumption rate denotes the proportion of electricity generated by the PV-system directly consumed by the household. In other words, instead of depending on grid power, the household utilizes the energy their PV-system produces. Equation 4.4 shows the self-consumption s, defined as the solar energy used directly E_{DU} and used for charging the battery E_{BU}, as a percentage of the overall produced PV energy E_{PV}.

$$s = \frac{E_{DU} + E_{BC}}{E_{PV}} \tag{4.4}$$

On the other hand, self-sufficiency refers to the percentage of the household's total electricity needs met by their own PV-BESS. This means that the household is not relying on energy from the grid at all. A higher self-sufficiency means that the household is more independent and less reliant on the grid, which can be especially useful during power outages or when there are grid disruptions. Equation 4.5 shows the self sufficiency d, defined as the solar energy used directly E_{DU} and the energy discharged from the battery E_{BD} as a percentage of the overal produced PV energy.

$$d = \frac{E_{DU} + E_{BD}}{E_L} \tag{4.5}$$

Running the simulation over one year yields the result that the self-sufficiency is equal to 58% and the self-consumption rate is equal to 83% for a household with a 15 kWh battery. The charge and discharge cycle during a typical sunny day is illustrated in figure 4.4, with 10 minutes resolution. As shown, the battery initially discharges until it reaches its lower limit on SOC. Once the battery is fully depleted, the household draws electricity from the grid to meet its domestic consumption. Excess solar energy is used to charge the battery as the sun rises, and any surplus power is exported to the grid. The shape of the curve can be modified by adjusting the size of both the PV system and the battery.

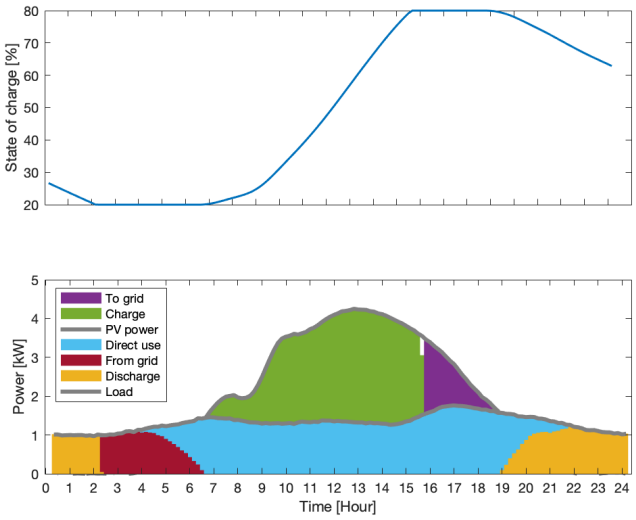

Figure 4.4: The figure illustrates the energy consumption activities of a house equipped with a PV-BESS during a sunny day.

Likewise, figure 4.5 depicts a more cloudy day where the solar energy generated is sufficient to meet the domestic energy needs for a significant portion of the day. However, no surplus electricity is exported to the grid.

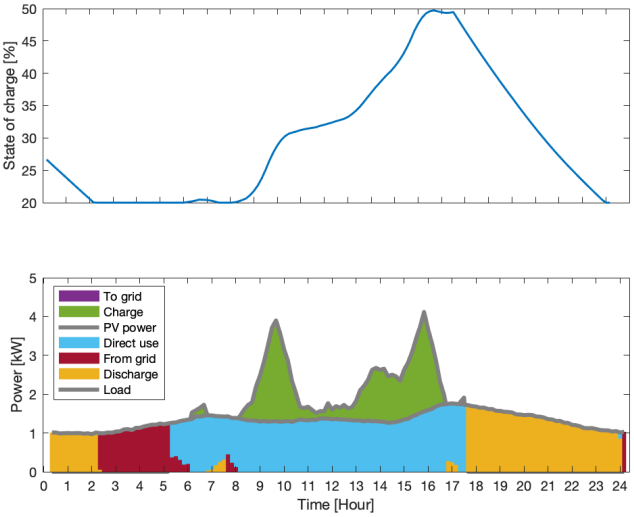

Figure 4.5: The figure illustrates the energy consumption activities of a house equipped with a PV-BESS during a cloudy day.

Simulation

The figure below illustrates the capacity decrease for a battery in a residential PV-BESS. The battery is charged when the solar production exceeds the domestic consumption. The C-rate is set to one, and the DOD varies following the difference between produced electricity and domestic consumption. The SOH is again set to range between 70% and 80%. However, it is likely that the SOH could go lower as the operation of the battery does not serve a critical function. In this case, the models show a higher agreement level than the CS-BESS. The battery can be used for three to seven years.

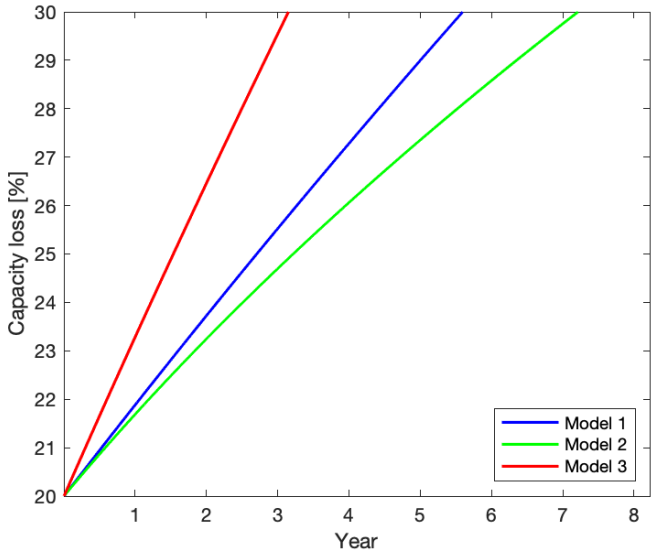

Figure 4.6: The figure illustrates the capacity loss of a battery in a residential PV-BESS.

At the same time, the resistance increases by 32%. For a lithium-ion 21700 battery this means that the internal resistance increases to 264 mΩ. Given the size of the battery, an active cooling system should not be necessary.

4.4 Pack Degradation

Based on the computations above, it is reasonable to have a battery capacity of approximately 510 kWh for a CS-BESS. Similarly, the size of a residential PV-BESS can be around 15 kWh to achieve relatively high self-sufficiency. Assuming a typical lithium-ion 21700 cell weighs 60 g and has a rated Watt-hour of 17.76, the total weight would amount to 2,000 kg for the former scenario and 50 kg for the latter. However, the ad hoc calculations provided above only serve to show reasonable battery sizes for different applications. In the decision-making process, calculations should be complemented with optimization techniques to minimize overall costs. Also, more advanced simulation software can be used.

Simulating battery degradation at the cell level and extrapolating the results to represent the aging of a battery pack is based on several underlying assumptions. Initially, when individual battery cells are combined into a pack, they undergo varying stress conditions. This is attributed to the inherent disparities among the cells and potential differences in current drawn, leading to variations in their state of charge levels. To address this, cell balancing becomes imperative. The extent of cell balancing depends on the sophistication of the BMS employed. As described in section 2.2, a sophisticated BMS actively balances the SOH of the cells, while a less advanced BMS restricts the capacity of the entire series of cells to match that of the weakest cell. In this paper, it is assumed that the battery packs are equipped with a sufficiently advanced BMS. Additionally, it is assumed that the battery pack is equipped with a thermal system to ensure the heat is uniformly distributed.

Figure 4.7 shows the two scenarios' calendar and cyclic aging disposition. Since both batteries are idle for long periods, calendar aging prevails. However, cyclic aging influences the CS-BESS to a greater degree, as the battery is operated more with a higher DOD.

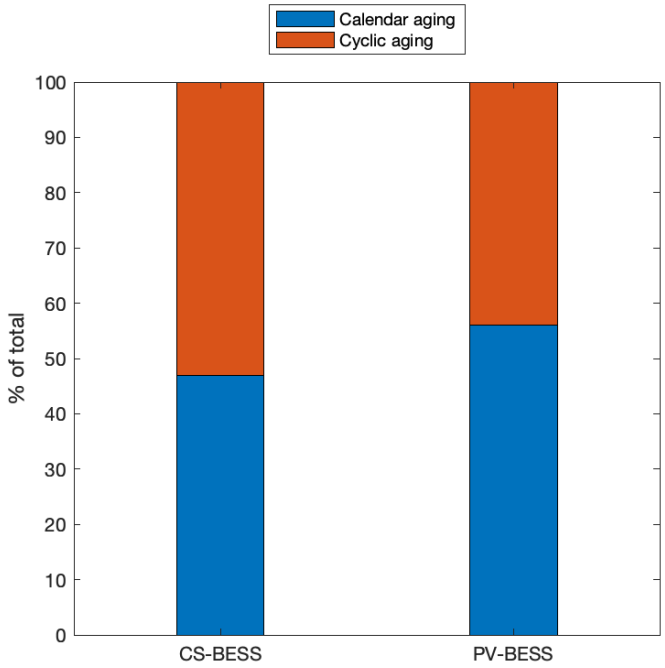

Figure 4.7: The figure illustrates how calendar and cyclic aging contribute to the overall capacity loss.

4.5 Chapter Summary

Most established models that address the aging of lithium-ion battery cells adopt a semi-empirical approach. Therefore, the accuracy and reliability of these models rely on the quality of experiments and the precision of the underlying physical relationships. The studies cited in this research employ a non-linear function of either time or ampere-hour throughput to depict a decrease in the rate of chemical reactions within the battery. In addition, all models utilize the Arrhenius equation to portray the exponential effect of aging resulting from elevated temperatures. However, concerning SOC, there is a lack of consensus on whether its influence on aging is exponential or linear. Similarly, the negative impact of high C-rates and DOD varies across different battery types and models.

Given the models presented above, it can be deduced that the usage characteristics of lithium-ion batteries impact the aging process and the change of the internal parameters. This work simulates different scenarios to display how batteries can be utilized in second-life applications. However, the RUL is vastly different for the different applications influencing the cost-benefit prognosis. For example, in the CS-BESS, the batteries are only expected to last 2-4 years. On the other hand, in a residential PV-BESS, the batteries are expected to last for 3-7 years. At the same time, the internal resistance increases by up to 32%, which causes significant heat losses.

5 Cost analysis

The chapter presents the main drivers of the costs of second-life EV batteries. Then the costs associated with stationary energy storage applications and configurations are outlined, encompassing the BMS, power electronics, and thermal system. Additionally, the benefits of second-life batteries in stationary applications are briefly explained, recognizing that they are highly contingent on the specific situation.

5.1 Cost of Second-life Battery

Only a few marketplaces are available for second-life EV battery packs and modules. These commercial intermediaries typically operate at a local level and are often characterized by limited liquidity and a low degree of standardization. Considering these factors, it is difficult to establish average prices for reused batteries, particularly on a global scale. The price variation depends on factors such as the specific battery type, its availability, and who the buyer is. Furthermore, the RUL of the battery and the extent of testing and disassembly conducted after its initial use influence the price. Despite these complexities, the cost of second-life EV batteries is generally estimated to fall within the range of 500-1,500 SEK/kWh.[1]

Presently the re-manufacturing of degraded EV batteries is a labor-intensive and costly process. Despite this, it is conceivable that a higher degree of automation will pervade the industry in the near future. In [19], a comprehensive overview of the disassembly process is presented. It is divided into sequential steps and evaluated based on the feasibility of automation and the importance of automating the corresponding disassembly operation. The findings suggest that automating the unscrewing process is advisable, while the lifting should be performed manually. The table below shows the cost of direct reusing an EV battery and re-manufacturing a battery from modules.

Table 5.1: Time (hours) of activities for direct reuse and module reconfiguration.

Operation	Direct reuse	Module reconfiguration
Physical inspection	0.5	0.5
Battery dismounting into modules	-	9
Test preparations	1	3.6
Battery test	24	24
Reassembling	1	9
Total	26.5	46.1

The testing phase is the most time-consuming stage of the battery re-habitation process, estimated to take 24 hours for a single EV battery [46]. This duration is due to the requirement of conducting both a capacity test and a pulse test. In addition, the testing involves discharging

[1] Initially stated in euro, the prices have been converted to SEK using a currency exchange rate of 11 SEK per euro.

the battery at different C-rates and durations while also adjusting the temperature. Thus the battery has to acclimate accordingly. Test procedures for lithium-ion battery packs developed for propulsion systems in road vehicles are provided in ISO 12405.

5.2 Battery Configuration in Stationary Applications

The costs associated with batteries in stationary applications vary significantly depending on specific circumstances and user requirements. Chapter 2 presents a general framework for using second-life batteries in different applications. The options are direct reuse and refurbishment from modules or cells. Each option has its advantages and disadvantages concerning performance, reliability, and costs.

In the context of second-life batteries, the BMS plays a crucial role in ensuring the safe operation of individual cells within the prescribed voltage range. When combining batteries from different manufacturers to form a new BESS, the BMS must ensure that all cells are charged and discharged at equal voltages. For instance, if two cells have SOC levels of 15 Ah and 25 Ah, the battery will be considered discharged once the lower-capacity cell is exhausted. This results in the underutilization of the larger capacity cell by 10 Ah. Addressing this issue is particularly challenging for non-uniform batteries with varying chemistries and SOH. Previous studies have proposed methods to overcome these challenges [47], although implementing them often requires additional electronic equipment, contributing to overall costs. Apart from the requirements on the performance of the BMS, the BMS topology also impacts the cost of the solution as it can be centralized, modular, or distributed [48]. The figure below provides a framework for different configurations of second-life batteries in stationary applications.

- **Stacking battery packs:** Stacking battery packs has the advantage of not being affected by the module distribution within the battery pack, allowing the packs to be stacked regardless of the degree of integrated or modular design. This approach requires minimal modification and can utilize the internal heating and cooling of the battery pack. Moreover, reusing batteries on pack level is more accepted by original equipment manufacturers as the product is less manipulated, reducing the risk of failure [19]. The main disadvantage of stacking battery packs is that the worst-performing module or cell impacts the system's performance. Additionally, modifying the pack's shape involves additional costs, and maintenance is expensive due to low flexibility.

- **Refurbished battery made from used modules:** Creating a new battery pack from refurbished modules allows the selection of the best modules from the original pack. This gives greater flexibility regarding the battery pack's dimensions [44]. However, the worst-performing cell affects the module performance, and the thermal management system needs to be replaced. Regarding the BMS it has to be designed for the new application. Some components of the original battery package, such as the housing, will not be used, while new components will be added, which increases cost and complexity.

- **Refurbished modules made from used cells:** Designing new battery packs at cell level enables selecting the best cells, considerably reducing the risk of incorporating damaged cells. This approach offers the most significant degree of flexibility regarding system size and shape. However, a significant disadvantage is that numerous components, such as covers, cooling plates, bus bars, and sensors, must be replaced and discarded, resulting in increased overall costs [15]. Additionally, there is a high risk of damaging the cells during disassembly.

CS-BESS
In the case of a CS-BESS, calculating the profitability is complex and the investment decision carries a significant risk of sunk costs, as indicated by [41]. The main costs involve the battery, installation of additional charging points, power electronics and thermal management system. A more elaborate assessment of the costs should also include costs of maintenance and depreciation's.

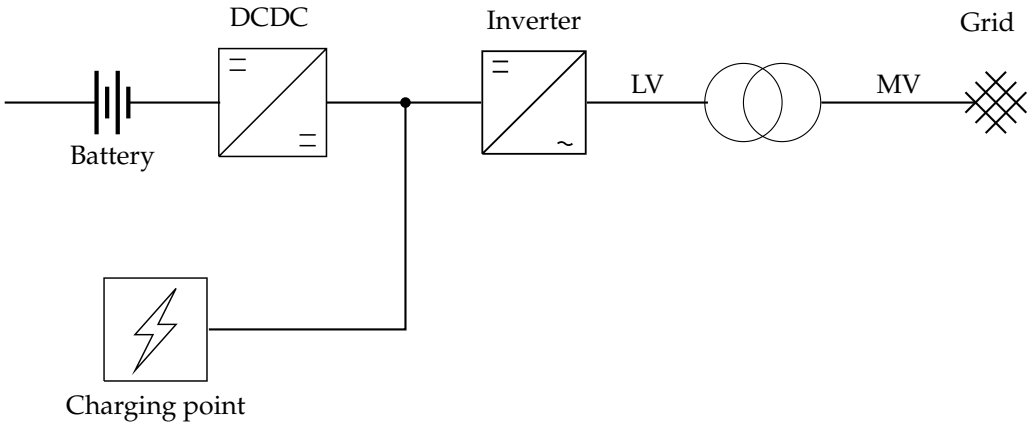

Figure 5.1: The figure illustrates a typical CS-BESS topology.

Figure 5.1 illustrates the system topology. For the battery to function as an energy buffer, a DC-DC converter is required in addition to the existing inverter. As stated in Chapter 4, in the CS-BESS, the battery should have a capacity of 510 kWh. This is more than most EV battery packs; therefore, multiple batteries must be stacked. The critical question that must be addressed is whether the batteries should be directly reused or refurbished at the module or cell level. The first option is the cheapest, while the latter entails more reliability at a higher cost. Other questions relate to reusing the BMS and thermal management system. Given that it is improbable that the batteries comprising the new CS-BESS have identical cell types and chemistries, a new BMS will likely be necessary. The question then becomes which BMS topology is the most advantageous and how the cell balancing should be conducted.

Assuming that the battery system costs 1,000 SEK/kWh, the cost multiplies to 500,000 SEK for the CS-BESS. Adding to this is the DC-DC converter. However, since multiple battery packs or modules will comprise the BESS, these will likely be connected in parallel. In this case, multiple converters might have to be connected to avoid developing undesired power flows between the individual battery packs [20]. In light of this, a cost of 100,000 SEK is added for the power electronics. It is assumed that the storage cost is negligible.

The costs of a CS-BESS should be related to the main alternative, which is to expand the grid to ensure the power supply. The cost of expanding the grid connection for an EV charging station depends on various factors, such as the distance to the nearest power source or transformer and legal processes. A rough cost is given in [49] where it is estimated to be between 100,000 and 200,000 SEK per kilometer for medium voltage. The estimate also depends on the type of electricity transfer, overhead electricity lines, or underground cables. The expanded grid connection will be utilized for at least 20 years, while the battery system must be replaced within four years. Thus, the cost of CS-BESS exceeds the cost of expanding the grid expansion annually. Considering this, implementing EV batteries in charging infrastructure can be justified as a temporary solution, thereby utilizing the inherent mobility of batteries and avoiding significant upfront investments.

PV-BESS
A cost analysis for a residential PV-BESS has previously been performed in [50]. The payback time for a residential establishment with solar panels usually falls in the 10-15 years range. The cost savings and revenue generated after this point translates to end-user profit. A solar panel's performance warranty will typically guarantee 90% production at ten years and 80% at 25 years. A simple example is given in [51], a PV system covering a relatively large area, producing 9,500 kWh per year, costs approximately 180,000 SEK. With a tax credit of 19.4%, the upfront cost is 144,000 SEK. Given a disposition between direct use and sold electricity, the cost savings are around 11,000 SEK per year. This translates to a payback time of 13 years.

Adding a stationary battery allows the user to store energy when the production exceeds the production. The battery size is usually in the range of 5 kWh to 15 kWh, which means that the maximal stored energy is less than the daily consumption of a residence. Although storing energy on a seasonal basis would be desired, this would necessitate too large batteries. As described in Chapter 4 the size of the battery decides self-sufficiency and self-consumption. Integrating a stationary battery into the home PV system changes the economic outlook. A battery system must be coupled with dedicated power electronics such as a DC-DC converter and a bidirectional battery inverter, allowing the battery to charge and discharge. Difference typologies can be selected, and the system can either be AC-coupled or DC-coupled. The choice impacts overall efficiency and flexibility. The illustration below shows a typical topology. A Maximum Power Point Tracking (MPPT) is needed to regulate the charging of the battery from the solar panels by adjusting the charging voltage and current. This is essential because the output of solar panels can vary depending on factors such as temperature and shading.

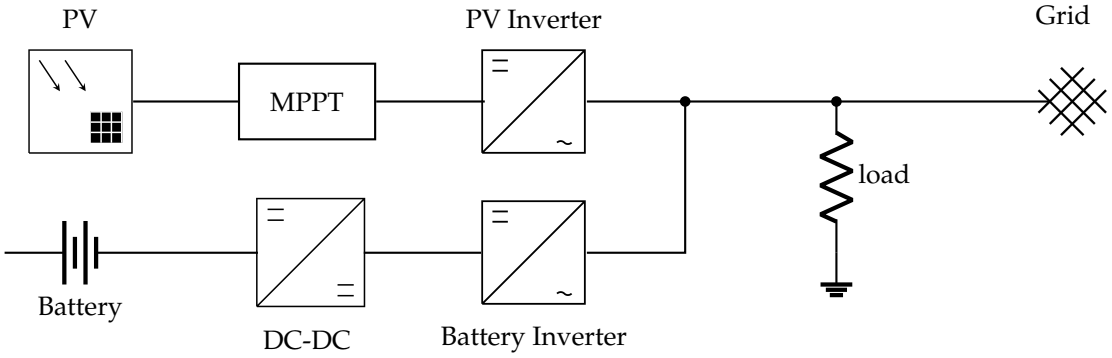

Figure 5.2: The figure illustrates a typical topology for a residential PV-BESS.

Previous studies have examined the expenses and advantages associated with installing a stationary battery in conjunction with a home PV system, as noted in [52] and [53]. However, most research conducted on this topic in a European context focuses on Germany, which has the largest battery storage market in Europe, with a capacity of 1.3 GWh in 2021. In Sweden, only one out of every 40 installed residential PV systems has an additional stationary battery. This is explained by the fact that surplus electricity can be sold at a price similar to the market rate, making it financially ill-advised to store energy [54]

Building on the same scenario as presented in the previous Chapter 4, a residential house has a yearly electricity consumption of 9,500 kWh. The house is equipped with solar panels covering an area of 45 m^2. Simulating the system with solar radiation data, the total production during one year equals 8,000 kWh. Nevertheless, the energy obtained from the battery is 1,800 kWh. Assuming a minor difference between purchased and sold electricity prices, this only adds cost savings of 900 SEK per year.

Residential PV systems usually operate at 24 or 48 Volts, the same as in many EV battery pack modules, making integrating second-life battery modules easier. However, activities such as dismantling and testing still need to be performed. As deducted in the previous chapter, a 15 kWh battery is suitable for residential energy storage. Regarding the cost, it is assumed that the price per kWh is 1,200 SEK/kWh, slightly higher than in the case above; the price for the entire system becomes 24,000 SEK. Adding to this is a power inverter and BMS estimated to cost 2,000 SEK. Given that the battery generates special revenues of 900 SEK per year, and neglecting the cost of storage and passive cooling, it takes 26 years to generate incomes equivalent to the cost of the battery storage system. However, the investment will not generate profit as the battery has an RUL of 3-7 years and will need replacement. The main reason is that the price of sold electricity in Sweden is comparatively high, and the micro-producers receive a tax reduction below 30,000 kWh. Regardless, the batteries are beneficial in non-monetary aspects such as island production and providing households with electricity during blackouts.

6 Discussion

This chapter starts with a brief summary of the findings, followed by an aggregation of some critical insights. Subsequently, it highlights certain obstacles to deploying second-life batteries on a large scale, such as performance uncertainties and data management. Finally, the section titled "sources of errors" presents some scientific limitations that needs to be considered.

Key Findings

- Despite many years of research, understanding and modeling the battery aging process remains an area of ongoing research. Presently, semi-empirical modeling is the most widely accepted technique, as it provides reasonably accurate predictions at a low computational cost. However, with advancements in computational technology and discoveries in machine learning and artificial intelligence, physical modeling can be utilized to understand the aging process better.
- The upfront costs of acquiring a degraded EV battery impact the economic evaluation of integrating degraded EV batteries into stationary applications significantly. As outlined in Chapter 5, the costs are increased by the labor-intensive process of dismantling and testing. However, the purchase price could be substantially reduced if the remanufacturing process becomes more automated and standardized.
- The configuration of new battery packs plays a crucial role in the overall costs and flexibility of the stationary storage system. For instance, stacking degraded EV battery packs to form a new energy storage system entails minimal waste but offers a low degree of customization concerning dimensions and performance.
- An energy management system (EMS) is necessary for optimal operation in a BESS. The EMS should account for forecast errors, internal battery parameters, system topology, and thermal concepts. Previous research has emphasized that optimization is essential for determining the profitability of various applications such as grid-scale peak shaving and spot-price arbitrage.
- As described in Chapter 5, the BMS plays a crucial role in reusing EV batteries. Granting third-party access to the data and information of the internal parameters reduces the required effort to evaluate the battery significantly. Also, degraded batteries with various characteristics may demand a more advanced BMS with active balancing capabilities, which entails additional electronics costs.

6.1 Modeling the Degradation of Lithium-ion Batteries

This thesis aims to investigate the use of EV batteries in stationary applications once they have reached the end of their initial life cycle. The batteries' RUL is crucial for the potential benefits in different scenarios. This study employs multiple aging models to understand how batteries age under different conditions comprehensively. Although the battery aging

models share certain common elements, they vary considerably. Moreover, technical and economic aspects are included to provide a complete picture of the current situation and make future predictions.

The outcomes of the RUL estimation presented in Chapter 4 suggest that the residential PV-BESS has the most extended lifespan. This is an expected finding because the battery storing excess solar energy production is not subjected to daily charging and discharging cycles due to the weather conditions. On the other hand, the CS-BESS is frequently used with more demanding usage characteristics, resulting in an accelerated aging process in capacity and resistance. Furthermore, it should be noted that the size of the battery pack impacts the stress factors, so oversizing batteries can extend their lifespan.

The cost analysis in Chapter 5 brings up essential aspects of acquiring second-life EV batteries and modifying the product to suit various stationary applications. The cost analysis in this paper suggests that implementing a stationary battery as a residential PV-BESS is seldom economically profitable. This is due to the relatively high price of selling energy to the electricity trading company. Albeit, micro-producers with the ability to use solar energy achieve a certain level of self-resiliency in case of blackouts or in case of other unexpected events that impact the grid supply. The cost of a CS-BESS should be compared with expanding the grid infrastructure to meet the power demand. As a grid expansion is expensive and might take a prolonged time to install, second-life batteries should be a solution. Furthermore, batteries' inherent modularity and portability facilitate the assembly of a suitable large battery pack placed in strategic locations.

6.2 Cost of Reusing Second-life EV Batteries

The market for second-life EV batteries lacks volume and liquidity and has a local presence. Additionally, the low degree of standardization entails that the prices vary significantly. This brings a high degree of uncertainty for the customers as the quantity and price of new batteries can not be accurately forecasted.

Aside from the market conditions, the cost of disassembling and testing EV batteries heavily impacts the overall cost. Moreover, this process is, to a large extent, manual, and numerous safety measures must be followed. For example, lithium-ion batteries have cutoff voltage limits to ensure a stable working range. Nevertheless, a discharged EV battery may have a voltage above 200 and plenty of power to deliver, and the SOC can only be accurately estimated after it has been tested. Therefore, safety is essential when manipulating a battery pack. Moreover, as lithium is a highly reactive and flammable element, products consisting of lithium are classified as dangerous goods. This causes difficulties with respect to transportation and pack management, which further adds to the cost.

As presented in the previous chapter, testing a second-life EV battery may take up to 24 hours. In addition, these tests encompass various charge and discharge operations with different external conditions. Apart from the costs of test equipment and labor, the tests negatively impact the batteries. However, automation and technologies such as spectroscopy might simplify the test procedure.

6.3 Battery Data

A practical barrier to implementing second-life batteries in stationary applications relates to data sharing, which ties to the historical usage patterns of the battery and the evolution of the internal parameters. The most important internal parameters are the number of full equiva-

lent cycles that the battery has undergone and the SOH of each cell for capacity and internal resistance. Knowledge of a battery's internal parameters is crucial for estimating its RUL, optimizing operational efficiency, and ensuring the safe handling of the battery. However, granting third-party access to the BMS, including the CAN-Matrix of a battery, means important software is also disclosed, such as SOH and SOC prediction algorithms. Vehicle manufacturers do not want to share this highly sensitive immaterial property with competitors. Despite this, various methods have been proposed to overcome these data-sharing obstacles, such as digital passports that can bridge information gaps. However, a study by [55] highlights key barriers to implementing such a system, including concerns over data security, storage and processing, and stakeholders' reluctance to share information due to immaterial requirements and property concerns.

6.4 Sources of Error

The numerical results of the case studies in this paper demonstrate significant differences in the aging models of lithium-ion batteries that affect their capabilities and limitations. For example, many models cannot accurately capture the impact of all possible stress factors, including C-rate, temperature, SOC, and DOD. Additionally, most models are designed for automotive applications and are limited to charge and discharge profiles specific to those use cases, resulting in a studied SOH range of typically 100% to 70%. As the number of energy storage systems increases, it will be essential to investigate the aging process of batteries in specific applications, including first and second-life batteries.

A critical parameter that heavily impacts the outcome of this thesis is the lower bound on the SOH of a battery, which is decided concerning the performance and breakdown characteristics of the battery. To this day, different views exist on when a battery should be declared depleted of utility. Some studies claim that a battery can be used until reaching 40% SOH, while others claim that 60% is a determined limit. Apart from the low capacity, two indications of an aged battery are when the self-discharge rate is high and the battery gets noticeably hot when charging or discharging. Despite this, the lower bound on SOH can likely be lower in specific applications. This remains to be studied.

7 | Conclusion

This chapter contains a summary of the purpose and research questions. Then, the results are discussed in relation to the main objectives of the thesis. Finally, the last two sections discuss the academic implications of the thesis and future work by putting the work in a broader context. This serves to answer the question of who can benefit from the scientific progress and what remains to be investigated.

7.1 Concluding Remarks

This paper investigates the technical and economic feasibility of implementing degraded EV batteries in stationary applications. Two realistic scenarios are created and simulated to determine how degraded EV batteries behave in different stationary applications. The RUL serves as a critical indicator of the duration of which the benefits emerge in each scenario. The first scenario involves a CS-BESS. It is assumed that the power supply of the charging station is exceeded multiple times per week. Implementing a BESS is a possible solution, but the results indicate that the battery SOH will reach the lower bound within four years. The second scenario involves a residential PV-BESS. In this scenario, it is assumed that the battery is used more beneficially, fluctuating around 50% SOC. In this scenario, the SOH reaches the lower bound in seven years.

Although the simulations use accurate data to the most significant extent possible, i.e., regarding solar radiation, energy consumption, and electricity prices, it is essential to note that the scenarios are established based on numerous assumptions. Many of which revolve around specific use cases and customer requirements. Thus, it is essential to note that the results are highly contingent on the use case, and it is suggested that a thorough analysis using the aging mentioned above framework is performed before indulging in energy storage projects with second-life batteries. Furthermore, the two scenarios targeted in this thesis only constitute a limited share of the available stationary applications. Therefore, more scenarios must be considered to understand better the opportunities and limitations of implementing second-life batteries in stationary applications. This includes stationary applications on different transmission and distribution grid levels for peak shaving, frequency regulation, and other applications. Also, other behind-the-meter applications can be examined, such as uninterrupted power supplies.

7.2 Academic Implications

This work proposes a battery aging framework to estimate the RUL of second-life batteries in different stationary applications. The framework utilizes well-established battery aging models from the literature. The usability and limitation of the modes are explained, as it is clear that all of the models have a high degree of explanation in some scenarios. As most battery aging models are developed for automotive applications, it is noted that the models do not work as well for stationary applications. This is due to the sheer fact that the charge and discharge patterns differ and that the SOH is generally lower. However, the framework

can be used to predict the RUL of batteries in stationary applications.

In addition to the RUL estimation, this thesis devotes a chapter to analyzing the costs of second-life batteries in the context of stationary storage. Although no new results are presented, numerous monetary and practical obstacles are highlighted. Many of which derive from the BMS and data sharing.

7.3 Future Work

As mentioned in chapter 3, to this day, most established battery aging models found in the literature have been developed to optimize operations and predict the RUL for hybrid electric vehicles. Therefore, the test procedures emulate common operations for the specific type of vehicle. This narrows down to a distinct range of equivalent full cycles, stress factors, and SOH. Using these models for other applications should be done with prudence. However, vehicle manufacturers have likely developed more advanced models for describing battery systems and the relationship between the key variables. For strategic reasons, these models are not publicly available. Nevertheless, more experimental data and models will be available as the research field evolves. This opens up new possibilities for accurately describing the degradation process in first and second-life applications.

In addition, this thesis only uses semi-empirical models for describing the aging process. The reason is that semi-empirical models are computationally efficient and do not require vast data. However, with the development of more powerful and efficient microprocessors, electrochemistry-based models might receive increased attention in the upcoming future. Also, data-driven models can be investigated in the context of second-life batteries in stationary applications. However, the drawback is that this method requires large amounts of experimental data, which is expensive given the vast number of battery cell types, chemistries, functional characteristics, and other properties.

Bibliography

[1] H.-O. Portner, D. C. Roberts, H. Adams, C. Adler, P. Aldunce, E. Ali, R. A. Begum, R. Betts, R. B. Kerr, R. Biesbroek, *et al.*, *Climate change 2022: Impacts, adaptation and vulnerability*. IPCC Geneva, Switzerland: 2022.

[2] IEA, "Global ev outlook 2022," 2022.

[3] Y. Kotak, C. Marchante Fernandez, L. Canals Casals, B. S. Kotak, D. Koch, C. Geisbauer, L. Trilla, A. Gomez-Nunez, and H.-G. Schweiger, "End of electric vehicle batteries: Reuse vs. recycle," *Energies*, vol. 14, no. 8, p. 2217, 2021.

[4] J. Warner, *Lithium-Ion Battery Chemistries*. Elsevier, 2019.

[5] R. Harnden, "Lightweight multifunctional composites: An investigation into ion-inserted carbon fibres for structural energy storage, shape-morphing, energy harvesting & strain-sensing," Ph.D. dissertation, KTH Royal Institute of Technology, 2021.

[6] S. Zhong, B. Yuan, Z. Guang, D. Chen, Q. Li, L. Dong, Y. Ji, Y. Dong, J. Han, and W. He, "Recent progress in thin separators for upgraded lithium ion batteries," *Energy Storage Materials*, vol. 41, pp. 805–841, 2021.

[7] P. N. Halimah, S. Rahardian, and B. A. Budiman, "Battery cells for electric vehicles," *International Journal of Sustainable Transportation Technology*, vol. 2, no. 2, pp. 54–57, 2019.

[8] A. A. Habib, M. K. Hasan, G. F. Issa, D. Singh, S. Islam, and T. M. Ghazal, "Lithium-ion battery management system for electric vehicles: Constraints, challenges, and recommendations," *Batteries*, vol. 9, no. 3, p. 152, 2023.

[9] L. C. Casals and B. A. Garca, "Communications concerns for reused electric vehicle batteries in smart grids," *IEEE communications magazine*, vol. 54, no. 9, pp. 120–125, 2016.

[10] Y. Yang, P. Wang, G. Lu, H. Dong, F. Li, and Y. Suo, "The analysis of battery cooling modes of ev," in *Proceedings of the 5th international conference on electrical engineering and automatic control*, Springer, 2016, pp. 865–875.

[11] H. E. Melin, "State-of-the-art in reuse and recycling of lithium-ion batteries–a research review," *Circular Energy Storage*, vol. 1, pp. 1–57, 2019.

[12] T. Or, S. W. Gourley, K. Kaliyappan, A. Yu, and Z. Chen, "Recycling of mixed cathode lithium-ion batteries for electric vehicles: Current status and future outlook," *Carbon Energy*, vol. 2, no. 1, pp. 6–43, 2020.

[13] C. H. Illa Font, H. V. Siqueira, J. E. Machado Neto, J. L. F. d. Santos, S. L. Stevan Jr, A. Converti, and F. C. Corrêa, "Second life of lithium-ion batteries of electric vehicles: A short review and perspectives," *Energies*, vol. 16, no. 2, p. 953, 2023.

[14] G. Harper, R. Sommerville, E. Kendrick, L. Driscoll, P. Slater, R. Stolkin, A. Walton, P. Christensen, O. Heidrich, S. Lambert, *et al.*, "Recycling lithium-ion batteries from electric vehicles," *nature*, vol. 575, no. 7781, pp. 75–86, 2019.

[15] L. Canals Casals and B. Amante Garcıa, "Assessing electric vehicles battery second life remanufacture and management," *Journal of Green Engineering*, vol. 6, no. 1, pp. 77–98, 2016.

[16] T. Montes, M. Etxandi-Santolaya, J. Eichman, V. J. Ferreira, L. Trilla, and C. Corchero, "Procedure for assessing the suitability of battery second life applications after ev first life," *Batteries*, vol. 8, no. 9, p. 122, 2022.

[17] M. Shahjalal, P. K. Roy, T. Shams, A. Fly, J. I. Chowdhury, M. R. Ahmed, and K. Liu, "A review on second-life of li-ion batteries: Prospects, challenges, and issues," *Energy*, vol. 241, p. 122 881, 2022.

[18] Y. Yang, E. G. Okonkwo, G. Huang, S. Xu, W. Sun, and Y. He, "On the sustainability of lithium ion battery industry–a review and perspective," *Energy Storage Materials*, vol. 36, pp. 186–212, 2021.

[19] J. F. Hellmuth, N. M. DiFilippo, and M. K. Jouaneh, "Assessment of the automation potential of electric vehicle battery disassembly," *Journal of Manufacturing Systems*, vol. 59, pp. 398–412, 2021.

[20] H. C. Hesse, M. Schimpe, D. Kucevic, and A. Jossen, "Lithium-ion battery storage for the grid—a review of stationary battery storage system design tailored for applications in modern power grids," *Energies*, vol. 10, no. 12, p. 2107, 2017.

[21] G. Fitzgerald, J. Mandel, J. Morris, and H. Touati, "The economics of battery energy storage: How multi-use, customer-sited batteries deliver the most services and value to customers and the grid," *Rocky Mountain Institute*, vol. 6, 2015.

[22] S. Wang, C. Fernandez, Y. Chunmei, Y. Fan, C. Wen, D.-I. Stroe, and Z. Chen, *Battery system modeling*. Elsevier, 2021.

[23] L. Driscoll, S. de la Torre, and J. A. Gomez-Ruiz, "Feature-based lithium-ion battery state of health estimation with artificial neural networks," *Journal of Energy Storage*, vol. 50, p. 104 584, 2022.

[24] S. Wang, C. Fernandez, Y. Chunmei, F. Yongcun, C. Wen, D.-I. Stroe, and Z. Chen, *Battery System Modeling: The Science of Microfabrication*. Elsevier, 2021.

[25] T. Huria, M. Ceraolo, J. Gazzarri, and R. Jackey, "High fidelity electrical model with thermal dependence for characterization and simulation of high power lithium battery cells," in *2012 IEEE International Electric Vehicle Conference*, 2012, pp. 1–8. DOI: 10.1109/IEVC.2012.6183271.

[26] S. Cho, H. Jeong, C. Han, S. Jin, J. H. Lim, and J. Oh, "State-of-charge estimation for lithium-ion batteries under various operating conditions using an equivalent circuit model," *Computers & Chemical Engineering*, vol. 41, pp. 1–9, 2012.

[27] J. Vetter, P. Novák, M. R. Wagner, C. Veit, K.-C. Moller, J. Besenhard, M. Winter, M. Wohlfahrt-Mehrens, C. Vogler, and A. Hammouche, "Ageing mechanisms in lithium-ion batteries," *Journal of power sources*, vol. 147, no. 1-2, pp. 269–281, 2005.

[28] A. Barré, B. Deguilhem, S. Grolleau, M. Gérard, F. Suard, and D. Riu, "A review on lithium-ion battery ageing mechanisms and estimations for automotive applications," *Journal of Power Sources*, vol. 241, pp. 680–689, 2013.

[29] C. R. Birkl, M. R. Roberts, E. McTurk, P. G. Bruce, and D. A. Howey, "Degradation diagnostics for lithium ion cells," *Journal of Power Sources*, vol. 341, pp. 373–386, 2017.

[30] J. Schmalstieg, S. Käbitz, M. Ecker, and D. U. Sauer, "A holistic aging model for li (nimnco) o2 based 18650 lithium-ion batteries," *Journal of Power Sources*, vol. 257, pp. 325–334, 2014.

[31] J. Wang, J. Purewal, P. Liu, J. Hicks-Garner, S. Soukazian, E. Sherman, A. Sorenson, L. Vu, H. Tataria, and M. W. Verbrugge, "Degradation of lithium ion batteries employing graphite negatives and nickel–cobalt–manganese oxide+ spinel manganese oxide positives: Part 1, aging mechanisms and life estimation," *Journal of Power Sources*, vol. 269, pp. 937–948, 2014.

[32] K. Smith, M. Earleywine, E. Wood, J. Neubauer, and A. Pesaran, "Comparison of plug-in hybrid electric vehicle battery life across geographies and drive-cycles," National Renewable Energy Lab.(NREL), Golden, CO (United States), Tech. Rep., 2012.

[33] B. Xu, A. Oudalov, A. Ulbig, G. Andersson, and D. S. Kirschen, "Modeling of lithium-ion battery degradation for cell life assessment," *IEEE Transactions on Smart Grid*, vol. 9, no. 2, pp. 1131–1140, 2016.

[34] P. M. Attia, A. Bills, F. B. Planella, P. Dechent, G. Dos Reis, M. Dubarry, P. Gasper, R. Gilchrist, S. Greenbank, D. Howey, *et al.*, ""knees" in lithium-ion battery aging trajectories," *Journal of The Electrochemical Society*, vol. 169, no. 6, p. 060 517, 2022.

[35] H. You, J. Zhu, X. Wang, B. Jiang, H. Sun, X. Wei, G. Han, and H. Dai, "The lithium-ion battery nonlinear aging knee-point prediction based on sliding window with stacked long short-term memory neural network," in *2022 IEEE Intelligent Vehicles Symposium (IV)*, IEEE, 2022, pp. 206–211.

[36] A. Karger, L. Wildfeuer, D. Aygül, A. Maheshwari, J. P. Singer, and A. Jossen, "Modeling capacity fade of lithium-ion batteries during dynamic cycling considering path dependence," *Journal of Energy Storage*, vol. 52, p. 104 718, 2022.

[37] T. Raj, A. A. Wang, C. W. Monroe, and D. A. Howey, "Investigation of path-dependent degradation in lithium-ion batteries," *Batteries & Supercaps*, vol. 3, no. 12, pp. 1377–1385, 2020.

[38] I. Baghdadi, O. Briat, J.-Y. Deletage, P. Gyan, and J.-M. Vinassa, "Lithium battery aging model based on dakin's degradation approach," *Journal of Power Sources*, vol. 325, pp. 273–285, 2016.

[39] A. Cordoba-Arenas, S. Onori, Y. Guezennec, and G. Rizzoni, "Capacity and power fade cycle-life model for plug-in hybrid electric vehicle lithium-ion battery cells containing blended spinel and layered-oxide positive electrodes," *Journal of Power Sources*, vol. 278, pp. 473–483, 2015.

[40] G. F. Savari, M. J. Sathik, L. A. Raman, A. El-Shahat, H. M. Hasanien, D. Almakhles, S. H. A. Aleem, and A. I. Omar, "Assessment of charging technologies, infrastructure and charging station recommendation schemes of electric vehicles: A review," *Ain Shams Engineering Journal*, p. 101 938, 2022.

[41] S. Funke, P. Jochem, S. Ried, and T. Gnann, "Fast charging stations with stationary batteries: A techno-economic comparison of fast charging along highways and in cities," *Transportation Research Procedia*, vol. 48, pp. 3832–3849, 2020.

[42] F. Liberati, A. Di Giorgio, and G. Koch, "Optimal stochastic control of energy storage system based on pontryagin minimum principle for flattening pev fast charging in a service area," *IEEE Control Systems Letters*, vol. 6, pp. 247–252, 2021.

[43] M. S. Mastoi, S. Zhuang, H. M. Munir, M. Haris, M. Hassan, M. Usman, S. S. H. Bukhari, and J.-S. Ro, "An in-depth analysis of electric vehicle charging station infrastructure, policy implications, and future trends," *Energy Reports*, vol. 8, pp. 11 504–11 529, 2022.

[44] M. Anderman, "Assessing the future of hybrid and electric vehicles," *The xEV Industry Insider Report. Second Edition. Advanced Automotive Batteries (AAB). Oregon House/California, USA*, 2013.

[45] J. Weniger, T. Tjaden, and V. Quaschning, "Sizing of residential pv battery systems," *Energy Procedia*, vol. 46, pp. 78–87, 2014.

[46] L. Canals Casals, B. Amante Garcıa, and M. M. González Benıtez, "A cost analysis of electric vehicle batteries second life businesses," in *Project Management and Engineering Research, 2014: Selected Papers from the 18th International AEIPRO Congress held in Alcañiz, Spain, in 2014*, Springer, 2016, pp. 129–141.

[47] M. Einhorn, W. Guertlschmid, T. Blochberger, R. Kumpusch, R. Permann, F. V. Conte, C. Kral, and J. Fleig, "A current equalization method for serially connected battery cells using a single power converter for each cell," *IEEE Transactions on Vehicular Technology*, vol. 60, no. 9, pp. 4227–4237, 2011.

[48] M. Monhof, D. Beverungen, B. Klör, and S. Bräuer, "Extending battery management systems for making informed decisions on battery reuse," in *New Horizons in Design Science: Broadening the Research Agenda: 10th International Conference, DESRIST 2015, Dublin, Ireland, May 20-22, 2015, Proceedings 10*, Springer, 2015, pp. 447–454.

[49] K. Knezović, M. Marinelli, P. Codani, and Y. Perez, "Distribution grid services and flexibility provision by electric vehicles: A review of options," in *2015 50th International Universities Power Engineering Conference (UPEC)*, IEEE, 2015, pp. 1–6.

[50] M. Bruch and M. Müller, "Calculation of the cost-effectiveness of a pv battery system," *Energy Procedia*, vol. 46, pp. 262–270, 2014.

[51] N. Sommerfeldt, "Solar pv in prosumer energy systems: A techno-economic analysis on sizing, integration, and risk," 2019.

[52] C. N. Truong, M. Naumann, R. C. Karl, M. Müller, A. Jossen, and H. C. Hesse, "Economics of residential photovoltaic battery systems in germany: The case of tesla's powerwall," *Batteries*, vol. 2, no. 2, p. 14, 2016.

[53] M. Naumann, R. C. Karl, C. N. Truong, A. Jossen, and H. C. Hesse, "Lithium-ion battery cost analysis in pv-household application," *Energy Procedia*, vol. 73, pp. 37–47, 2015.

[54] E. Nyholm, *The role of Swedish single-family dwellings in the electricity system*. Chalmers Tekniska Hogskola (Sweden), 2016.

[55] K. Berger, R. J. Baumgartner, M. Weinzerl, J. Bachler, and J.-P. Schöggl, "Factors of digital product passport adoption to enable circular information flows along the battery value chain," *Procedia CIRP*, vol. 116, pp. 528–533, 2023.

Appendix

The calibrated parameters for the capacity loss and resistance increase are resistance in the tables below.

Appendix A

The parameters corresponding to model 1 are presented below.

	Capacity fade	**Power fade**
$\mathbf{a_1}$	8.314	8.314
$\mathbf{a_2}$	81480	57.52
$\mathbf{a_3}$	0.288	0.35
$\mathbf{a_4}$	158.28	112.92
$\mathbf{a_5}$	49.5	49.5
$\mathbf{a_6}$	-24.06	-24.06
$\mathbf{z}$	1	1

Appendix B

The parameters corresponding to model 2 are presented below.

	Capacity fade	**Power fade**
$\mathbf{a_1/b_1}$	137	$3.2 \cdot 10^5$
$\mathbf{a_2/b_2}$	420	$1.3674 \cdot 10^9$
$\mathbf{a_3/b_3}$	0.34	0.25
$\mathbf{a_4/b_4}$	9610	5.45
$\mathbf{a_5/b_5}$	3	$3.63 \cdot 10^3$
$\mathbf{a_6/b_6}$	-	9.9179
$\mathbf{a_7/b_7}$	-	1.8277
$\mathbf{a_8/b_8}$	-	0.25
$\mathbf{E_c/E_R}$	22406	51800
$\mathbf{CR_0}$	-	5

Appendix C

The parameters corresponding to model 3 are presented below.

	Capacity fade	Power fade
$\mathbf{a_1}/\mathbf{b_1}$	7.54	5.27
$\mathbf{a_2}/\mathbf{b_2}$	23.75	16.32
$\mathbf{a_3}/\mathbf{b_3}$	6976	5986
$\mathbf{a_4}/\mathbf{b_4}$	$7.348 \cdot 10^{-3}$	$2.153 \cdot 10^{-4}$
$\mathbf{a_5}/\mathbf{b_5}$	3.67	3.73
$\mathbf{a_6}/\mathbf{b_6}$	$7.6 \cdot 10^{-4}$	$1.521 \cdot 10^{-5}$
$\mathbf{a_7}/\mathbf{b_7}$	$4.081 \cdot 10^{-3}$	$2.798 \cdot 10^{-4}$

Appendix D

The table below shows the datasheet for a typical lithium-ion battery used in electric vehicles.

Li-Ion 21700	
Rated capacity	4800 mAh
Nominal Voltage	3.7 V
Wat-Hour Rating	17.76 Wh
Max. Operating Voltage Range	2.75V to 4.20 V
Max. Charge Voltage	4.2 V ±50 mV
Max. Charge Current	2400 mA
Standard Charge Current	960 mA
Internal Impedance	<200 mΩ
Weight	60 g

Appendix E

The figure illustrates the Simulink model used to simulate the aging process. The models consist of auxiliary blocks to calculate the state of charge and dissipated heat every hour. Also, subsystems are utilized for increased readability.

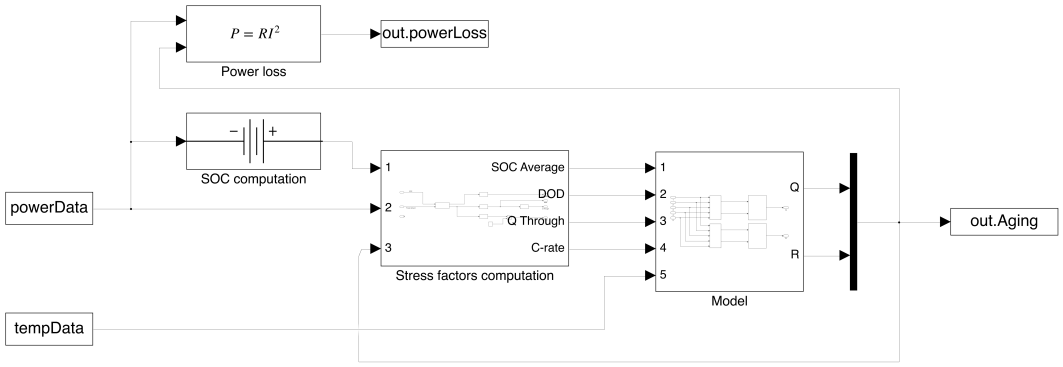

Appendix F

The figure shows the discharge curves of a lithium-ion 18650 battery. The data has been obtained from NASAs open data portal.

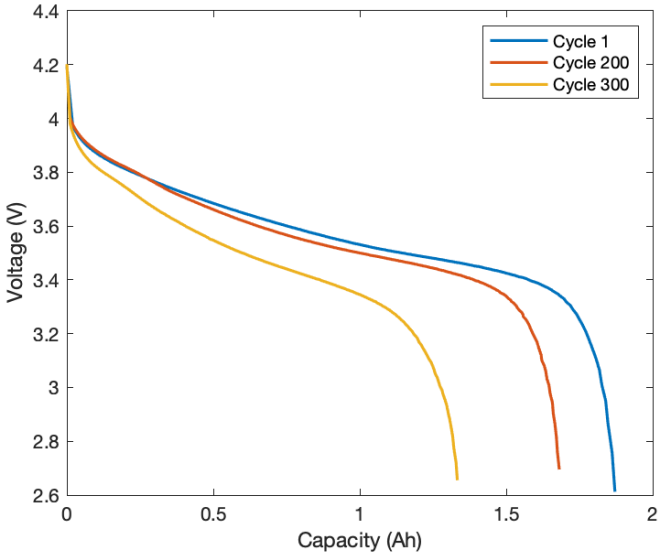

Appendix G

The figure shows the capacity fade of three lithium-ion 18650 batteries as a function of cycle number. The cut-off voltages are 2.7V, 2.5V, and 2.2V, respectively.